Mechanosensing in actin stress fibers revealed by a close correlation between force and protein localization

Julien Colombelli[1,*,‡], Achim Besser[2], Holger Kress[1,3], Emmanuel G. Reynaud[1], Philippe Girard[1], Emmanuel Caussinus[4], Uta Haselmann[1], John V. Small[5], Ulrich S. Schwarz[2] and Ernst H. K. Stelzer[1]

[1]Cell Biology and Biophysics, European Molecular Biology Laboratory (EMBL), Meyerhofstrasse 1, D-69117 Heidelberg, Germany
[2]University of Heidelberg, Bioquant, BQ0013 BIOMS Schwarz, Im Neuenheimer Feld 267, D-69120 Heidelberg, Germany
[3]Department of Mechanical Engineering, Yale University, New Haven, CT 06511, USA
[4]Biozentrum, Klingelbergstrasse 50/70, CH-4056 Basel, Switzerland
[5]Institute of Molecular Biotechnology Austrian Academy of Sciences (IMBA), Dr Bohrgasse 7, A-1030, Vienna, Austria
*Present address: Advanced Digital Microscopy, Institute for Research in Biomedicine (IRB Barcelona), Baldiri Reixac 10, E-08028 Barcelona, Spain
‡Author for correspondence (e-mail: julien.colombelli@irbbarcelona.org)

Accepted 6 January 2009
Journal of Cell Science 122, 1665-1679 Published by The Company of Biologists 2009
doi:10.1242/jcs.042986

Summary

The mechanics of the actin cytoskeleton have a central role in the regulation of cells and tissues, but the details of how molecular sensors recognize deformations and forces are elusive. By performing cytoskeleton laser nanosurgery in cultured epithelial cells and fibroblasts, we show that the retraction of stress fibers (SFs) is restricted to the proximity of the cut and that new adhesions form at the retracting end. This suggests that SFs are attached to the substrate. A new computational model for SFs confirms this hypothesis and predicts the distribution and propagation of contractile forces along the SF. We then analyzed the dynamics of zyxin, a focal adhesion protein present in SFs. Fluorescent redistribution after laser nanosurgery and drug treatment shows a high correlation between the experimentally measured localization of zyxin and the computed localization of forces along SFs. Correlative electron microscopy reveals that zyxin is recruited very fast to intermediate substrate anchor points that are highly tensed upon SF release. A similar acute localization response is found if SFs are mechanically perturbed with the cantilever of an atomic force microscope. If actin bundles are cut by nanosurgery in living *Drosophila* egg chambers, we also find that zyxin redistribution dynamics correlate to force propagation and that zyxin relocates at tensed SF anchor points, demonstrating that these processes also occur in living organisms. In summary, our quantitative analysis shows that force and protein localization are closely correlated in stress fibers, suggesting a very direct force-sensing mechanism along actin bundles.

Supplementary material available online at
http://jcs.biologists.org/cgi/content/full/122/10/1665/DC1

Key words: Mechanosensing, Stress fibers, Zyxin, α-actinin, Actomyosin contractility, Laser nanosurgery, Correlative microscopy, Viscoelasticity

Introduction

Mechanotransduction, or the mechanism by which cells convert mechanical stimuli into biochemical signals, is an essential element of many physiological and disease-related cellular processes, including cell adhesion, differentiation and migration. It also underlies many processes at the tissue level, including tissue homeostasis, wound healing and morphogenesis. At the interface between mechanics and biochemistry, cells need molecular sensors to detect mechanical movements, forces and tensions. However the list of well-established candidates is still very limited and the molecular details of mechanosensitivity are often elusive. Among the well characterized mechanosensitive mechanisms (Gillespie and Walker, 2001; Vogel and Sheetz, 2006), transmembrane ion channels are best known as mechanosensing structures that can detect and transduce external forces into electrical or chemical intracellular signals (Morris, 1998; Martinac, 2004). Focal adhesions (FAs) represent another type of 'mechanosensory organ'; they are mature sites of cell-matrix adhesion that are based on the transmembrane receptors from the integrin family. FAs incorporate a large number and diversity of compounds (Zaidel-bar et al., 2007), thus the precise description of force sensing and transmission in FAs is a great challenge. They assemble or reorganize directionally in response to external forces, as shown by single cell manipulation with micropipettes (Riveline et al., 2001; Guo and Wang, 2007), beads (Wang, 2007) or stretched substrates of adherent cells (Yoshigi et al., 2005; Kim-Kaneyama et al., 2005). Examples of mechanosensitive molecular mechanisms in FAs involve focal adhesion kinase (Mitra et al., 2005), paxillin in focal complexes (Zaidel-Bar et al., 2006) or the Src tyrosine kinase (Wang et al., 2005) and $p130^{Cas}$ (Sawada et al., 2006). Inside cells, internal movement of actin filaments can also be sensed by FAs through a slippage-clutch mechanism (Hu et al., 2007; Wang, 2007).

Recently, the FA component zyxin emerged as a potential mechanosensitive protein for cell adhesion. Cytoplasmic-nuclear shuttling (Nix and Beckerle, 1997) of zyxin indicated a putative link between mechanotransduction and transcription. At the macromolecular level, it responds to external cellular stretch by reorganizing along the cytoskeleton (CSK) to further reinforce it (Yoshigi et al., 2005), correlates with the actin retrograde flux at FAs (Guo and Wang, 2007) and its exchange rate in FAs changes

upon laser perturbation (Lele et al., 2006). These studies suggest a link between mechanical stimulus and zyxin behavior in FAs; however, no quantitative evidence of the relation between molecular forces and its intracellular translocation dynamics was reported. Moreover, zyxin interacts with the crosslinker protein α-actinin (Crawford et al., 1992; Reinhard et al., 1999; Li and Trueb, 2001) and is found in SFs, where its exact localization and its role are not yet understood.

SFs are actin bundles extending between FAs. Their formation and contractility are driven by non-muscle myosin II (Chrzanowska-Wodnicka and Burridge, 1996; Hotulainen and Lappalainen, 2006) by inducing bidirectional sliding of actin filaments. Actin-actin crosslinkers turn randomly sliding filaments into one-dimensional contractile bundles. The main linker within SFs is the α-actinin dimer, although other actin linkers are present (Pellegrin and Mellor, 2007). Myosin II and α-actinin localize complementarily and periodically along established SFs in sarcomere-like units (Peterson et al., 2004).

In this study, we demonstrate the close relationship between molecular localization of proteins and force propagation in SFs. We first show the fast tension release of SFs by laser nanosurgery and analyze their dynamics of retraction. Unexpectedly, our analysis indicates a strong mechanical coupling between SFs and the cellular environment. We introduce a theoretical model for the mechanics of SFs that we demonstrate to be in good agreement with the measured data. Stress distribution along FAs and SFs cannot be experimentally measured; however, our model allows the calculation of force propagation through the actin bundles.

We then perform a case study on the dynamics of zyxin in SFs and FAs and find a strong correlation between the computed forces

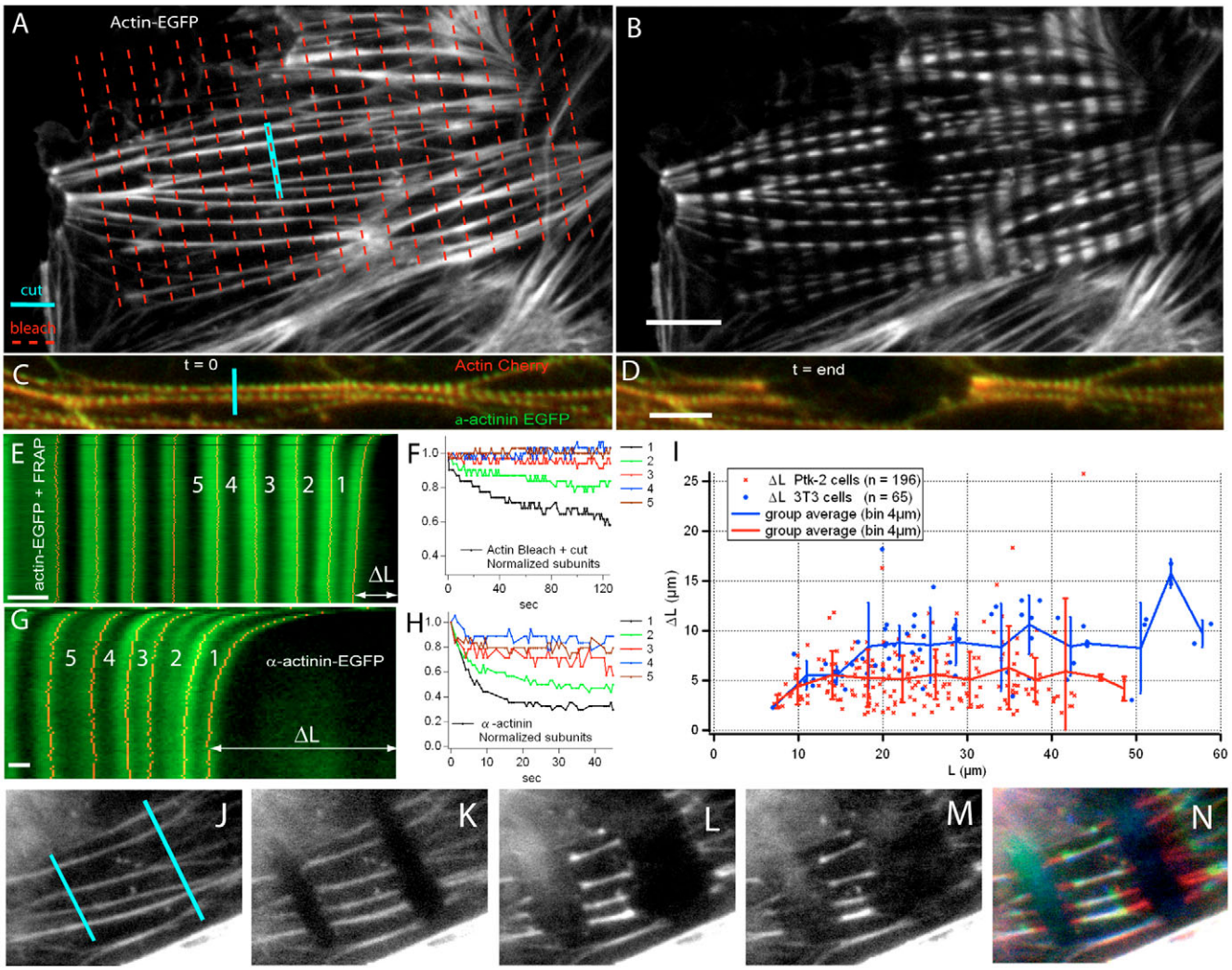

Fig. 1. Actin SF retraction after photobleaching and laser nanosurgery. (A) A 3 μm periodic laser pattern (dashed lines) bleaches across a Ptk-2 cell expressing actin-EGFP, perpendicularly to the SF axes. Laser dissection (blue lines) occurs between two stripes within 10 to 20 seconds after bleaching. (B) 120 seconds after cut. (C) SFs expressing actin-Cherry and α-actinin-EGFP. (D) 120 seconds after laser release. Note the stronger retraction at the tips. (E,G) Kymograph analyses of SFs from both experiments. The edge detection performed for further analysis of the stripes displacement is shown in red. Δ*L*, total retraction of the fiber after equilibration. (F,H) Normalized widths of five subunits closer to the cut tips, numbered according to kymographs. (I) Δ*L* as a function of the initial SF length *L*, measured in epithelial cells and fibroblasts. Segmented lines show mean values calculated over 4 μm intervals of the *x*-axis, bars show s.d. Δ*L* reaches a constant value for *L*>10 μm. (J-N) SF dissected simultaneously in two locations. The retraction occurs from both locations and is shown 2 seconds, 10 seconds and 60 seconds after cut in K, L and M, respectively. (N) Overlap of the three time points with red (K), green (L) and blue (M) shows no lateral movement of the fiber fragments as they retract along their original axis. Scale bars: 10 μm (B), 5 μm (D), 3 μm (E), 1 μm (G). See supplementary material Movie 1.

and its translocation dynamics. First, in response to tension release by laser nanosurgery and drug treatment, zyxin translocates away from SFs and FAs. By contrast, if we increase the mechanical load on single SFs with an atomic force microscope (AFM), we observe subsequent enrichment of zyxin within the pulled SFs in an acute and reversible manner. The further comparison between fluorescence distribution, correlative electron microscopy and force calculations shows that large amounts of FA-related proteins are recruited upon retraction of SFs along the plasma membrane, suggesting a new mechanism of adhesion formation by intracellular mechanical movements.

Of particular importance, nanosurgery of actin bundles in follicular cells of *Drosophila* egg chambers shows that zyxin responds similarly in vivo, with identical mechanosensitive dynamics. Altogether, our study suggests that SFs behave as prominent mechanosensing platforms able to detect intracellular forces with proteins that might have a much more prominent role than formerly appreciated.

Results

Retraction dynamics of SFs after nanosurgery

To determine the mechanical properties of SFs, we recorded their retraction after laser nanosurgery (Colombelli et al., 2005). We transiently transfected mammalian epithelial Ptk-2 and Swiss 3T3 fibroblasts with a G-actin-EGFP construct. Laser photobleaching allowed us to pattern SFs prior to cut (Fig. 1A,B) and to spatially resolve the displacement field during retraction (Fig. 1E,F). A 3 µm periodic pattern was printed perpendicular to the axis of the selected SFs before dissection (Fig. 1; supplementary material Movie 1). When cut, both basal semi-fibers retract over several microns whereas the number of fluorescent stripes is conserved within the typical equilibration time of about 1 minute. This indicates that depolymerization of SFs after cut was not observed.

First, we quantified the total retraction length ΔL of dissected semi-fibers (Fig. 1I) after equilibration. In both cell lines, we found ΔL to be independent of the initial length L. ΔL reached a plateau at about 5-6 µm in Ptk-2 cells (n=196 SFs) and 8-9 µm in Swiss 3T3 cells (n=65 SFs). By applying an edge detection to the time-space kymograph of a retracting SF (see Materials and Methods), we retrieved the time-dependent positions of the fluorescent stripes, shown as red curves in Fig. 1E. Stripes at the SF tip contracted widely as opposed to internal segments, further away from the cut, hence showing non homogeneous retraction along the SF. The corresponding time courses of the normalized stripe width $[w(t)-w_0]/w_0$, which is analogous to the strain in the fiber, are shown in Fig. 1F. The same experiments were also performed in Ptk-2 cells transfected to express α-actinin-EGFP (Fig. 1C-D; supplementary material Fig. S1). The natural striated pattern with periodic spacing of about 1 µm contracted in a similar manner to actin, with a similar compaction at the tip and constant retraction length ΔL for large fibers. Furthermore, we also released free segments of actin-EGFP SFs by cutting in two locations (Fig. 1J-N). We observed that their contraction occurred at the ends and along the initial SF axis, without lateral movement. From those observations, we conclude that released SFs retract non homogeneously and along a conserved axis.

A viscoelastic model provides quantitative insight into SF dynamics

To understand the previous observations, we analyzed the contraction dynamics of SFs by simulating them with a robust viscoelastic model. The sarcomeric structure of SFs is described as a linear chain of Kelvin-Voigt bodies (Fung, 1993). Each consists of a dashpot (friction coefficient γ_{int}) and a spring (stiffness k_{int}), connected in parallel (Fig. 2A). SF contractility is introduced with a further contractile element representing the myosin motor activity (contraction force F_m). These describe the internal mechanical properties. However SFs might also interact with the cellular environment. We therefore introduced an external harmonic restoring force with crosslinks of stiffness k_{ext}, as well as an external friction γ_{ext} due to the eventual viscous drag within the cytosol (summarized in Fig. 2). We then derived the central model equation for the displacement field $u(x,t)$ along the fiber (Eqn A5, Appendix 1). The model is finally reduced to four parameters (κ, δ, τ, τ_ε), each of which is a combination of the viscoelastic properties of the SF described above (see Table A1 in Appendix 1). κ is a measure for the degree of crosslink of a SF with external components; δ denotes the maximal contraction length of a sarcomeric unit. τ and τ_ε are equilibration times associated with internal and external

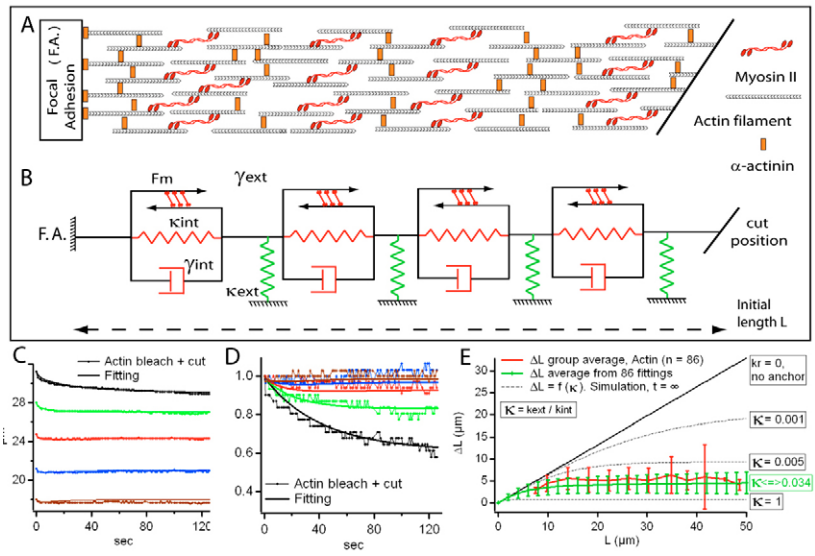

Fig. 2. Viscoelastic model used for data analysis. (A) Schematic view of the internal SF organization with actin, myosin II and the actin crosslinker α-actinin. (B) Representation of the viscoelastic model. In red, the elements of the internal contractile units: spring of stiffness k_{int}, dashpot of viscosity γ_{int} and contractile force F_m. In green, the external anchor springs of stiffness k_{ext}. Cytosolic friction is denoted by γ_{ext}. FAs and anchoring substrate are considered hard boundaries. Each kymograph was fitted with one set of model parameters. (C) Time course of the bleached stripes positions extracted from Fig. 1E overlapped with the fitted model curves. (D) Normalized stripe width overlapped to the corresponding model curves calculated from C. Colors correspond in C and D. One set of the four model parameters is sufficient to reproduce the non-homogeneous retraction of the whole SF. Fit values for parameters in C and D are (κ, δ, τ, τ_ε) = (0.067, 0.58 µm, 52 seconds, 0.0 seconds). (E) In red, the averaged total retraction $\Delta L(L)$, reported for Ptk-2 cells in Fig. 1I, shows a very good agreement with the model curve (green), averaged with 86 parameter sets extracted from the actin data (error bars show s.d.). The $\Delta L(L)$ model curve corresponds to an average crosslink ratio κ≈0.034 (see Appendix 1). For comparison, other ΔL curves are plotted (dashed lines) with κ=1, 0.005, 0.0001 and 0. Note that κ=0 would correspond to a free SF, i.e. with no external linkage (k_{ext}=0).

processes, respectively. Values for (κ, δ, τ, τ_ε) were retrieved by fitting the model to the kymograph traces. Fig. 2C shows a fit to a measured kymograph and Fig. 2D the corresponding time courses of the normalized subunit widths. The model reproduces very well the inhomogeneous contractions along the whole fiber and provides an excellent tool for a statistical analysis of the experimental data. In total, we obtained parameter sets (κ, δ, τ, τ_ε) from actin (n=86) and from α-actinin (n=34) transfected cells, as reported in Table A1. For actin-transfected cells the crosslink parameter amounts to κ=0.035±0.034 (mean ± s.d.). The maximal contraction length of a sarcomeric unit of initial width a=1 μm is δ=0.66±0.36 μm. Equilibration times τ and τ_ε are discussed in Appendix 1. The comparison in Table A1, shows that the parameters δ and τ_ε are rather independent of the transfected protein whereas the crosslink parameter κ=0.078±0.059 is significantly higher (Student's t-test: P_κ=0.0000014) and the time scale τ=15±11 seconds is significantly lower (t-test: P_τ=0.0029) in α-actinin-transfected cells. This suggests that α-actinin has an influence on the degree of crosslink of SF to the cellular environment.

Next, we calculated the stationary solution of the model, i.e. independently of the viscous contributions (see Table A1). We found that ΔL first increases linearly with L and then becomes independent of L for $L \gg a/\sqrt{\kappa} \approx 5.4$ μm (Eqn A10, Appendix 1). The value of the saturation level is $\delta/\sqrt{\kappa}$. Fig. 2E shows the contraction ΔL averaged over 86 model curves, each defined by one parameter pair (κ, δ). The predicted saturation level of $\Delta L(L$=50 μm)=4.5±2.5 μm is in good agreement with the experimental data shown in red for actin-transfected cells. The same analysis was performed on α-actinin-transfected cells (supplementary material Fig. S1). By contrast, the total contraction of an isolated, uncrosslinked fiber (κ=0) would be proportional to its length, as shown with a black solid line in Fig. 2E, and would not saturate. This indicates that an external crosslink of the SF, expressed by a non-vanishing κ, is required to model the saturation in ΔL, and therefore that SFs are strongly anchored to a subcellular element.

Zyxin distribution within FAs and SFs adapts to mechanical perturbations

We used Ptk-2 cells and Swiss 3T3 fibroblasts transfected with zyxin EGFP and actin cherry constructs to study zyxin dynamics in response to nanosurgery in SFs. Fig. 3A-I shows typical SFs in a double-transfected Ptk-2 cell that has been cut sequentially in different locations. First, we released a 14-μm-long centerpiece by two simultaneous laser cuts along the same bundle (Fig. 3B). After a 30-second contraction phase, we performed a second cut that dissected the fragment in its middle and a neighboring SF (Fig. 3C). This experiment revealed three translocation processes. After cut, zyxin dissociates from FAs and the dissected SFs, but in turn aggregates at distinct positions along the fiber fragments (supplementary material Movies 2 and 3). FAs connected to a cut SF experienced a quick loss of zyxin intensity, as shown in Fig. 3D,E,J (intensity profiles) and Fig. 3K (intensity over time). We quantified this loss according to the distance L, between the cut and the connected FA. In both cell lines, we found that the relative zyxin intensity loss is about 40% when cutting close to the FAs, but decreases with increasing L. The loss drops below 10% for L>30 μm (Fig. 3L). To test whether this intensity loss is related to a loss of force on the FA, we used our model to calculate the expected relative force loss δF_{rel} at FAs depending on the distance L. Indeed we found that δF_{rel} is an exponentially decaying function of L (Eqn A13, Appendix 1). Fig. 3L shows the average of δF_{rel} over 86 model curves, each defined by a specific value for κ retrieved previously from the fittings of Fig. 2. Therefore, the comparison of force loss with the relative zyxin intensity loss from FAs after cut suggests a close relationship between zyxin distribution and forces in FAs.

Zyxin intensity was also lost from the released SF fragment, suggesting a similar relationship in SFs. Within 5 seconds after cut, the typical sarcomeric pattern vanished from the SF, as shown in Fig. 3J (in the region 10-20 μm), and by comparing also Fig. 3D,E. Furthermore, we observed that zyxin relocalizes at random spots along the axis of cut SFs (Fig. 3B-I; supplementary material Movies 2 and 3). Interestingly, these zyxin foci are immobile. After formation close to the fiber tips (positions in Fig. 3C), their intensity steadily increases in time (Fig. 3K, red and green curves) as the SFs fragments contract. After cutting the middle part of the SF fragment, however, we observed a reversed movement of the two new fragments accompanied by a decrease of intensity in areas 1 and 2 in their vicinity. By contrast, the foci intensity increased continuously along external foci (areas 3 and 4, Fig. 3C) and a control cut neighbor SF. Notably, the free ends created by the last cut did not show systematic zyxin recruitment (Fig. 3I).

To correlate zyxin dynamics with the change of forces in the SF fragment, we simulated this sequence of laser cuts with the theoretical model and produced a kymograph of the tension within the fiber (Fig. 3O) and of the traction forces transmitted by the crosslinks to the substrate (Fig. 3P). We compared these with the measured kymograph of zyxin intensity along the SF fragment (Fig. 3M,N). The instantaneous loss of zyxin in the middle of the fiber correlated remarkably well with the loss of tension due to the first cut (+ and – in Fig. 3N,O), the increase of zyxin along the fiber axis due to traction forces exerted on the crosslinks (* in Fig. 3N,P; area 1 and 2 in Fig. 3C) and, after the second cut, the subsequent decrease of zyxin with the release of tension at the same location (× in Fig. 3N,P). These results therefore suggest that zyxin localizes where forces are applied along SFs and FAs.

Internal forces along SFs induce formation of nascent adhesion sites

To localize more precisely the new foci of zyxin recruitment after SF retraction, we performed correlative live fluorescent and transmission electron microscopy (TEM). A recent protocol allowed us to fix cells after live SF nanosurgery and prepare them for TEM (Colombelli et al., 2008). Fig. 4 shows the correlation between fluorescent distribution of basal-SF-actin cherry and EGFP zyxin after several SFs were cut. We compared the electron micrographs of the first three sections (50 nm thickness) around the cut area (Fig. 4), around control FAs and along their connected SFs (supplementary material Fig. S2). The two internal planes (Fig. 4C,D) clearly showed actin filaments and the morphology of the cut or intact fibers. The first section, corresponding to the region of the cell in contact with the glass coverslip, showed by contrast a very dense and localized signal. Fig. 4F-H shows clear similarities between distinct fluorescent signals and distinct TEM sections. A similar correspondence is found at the control FA (supplementary material Fig. S2) whereas no signal was detected below uncut SFs in the first section, (supplementary material Fig. S2). Zyxin thus relocalizes in the first section, at a maximum of 50 nm from the glass surface.

The striking similarity between a FA and the new zyxin foci after cut suggests that zyxin translocates to new adhesions along the retracting SF. To confirm this we monitored the fluorescent localization of vinculin, a core FA component, along SFs after cut.

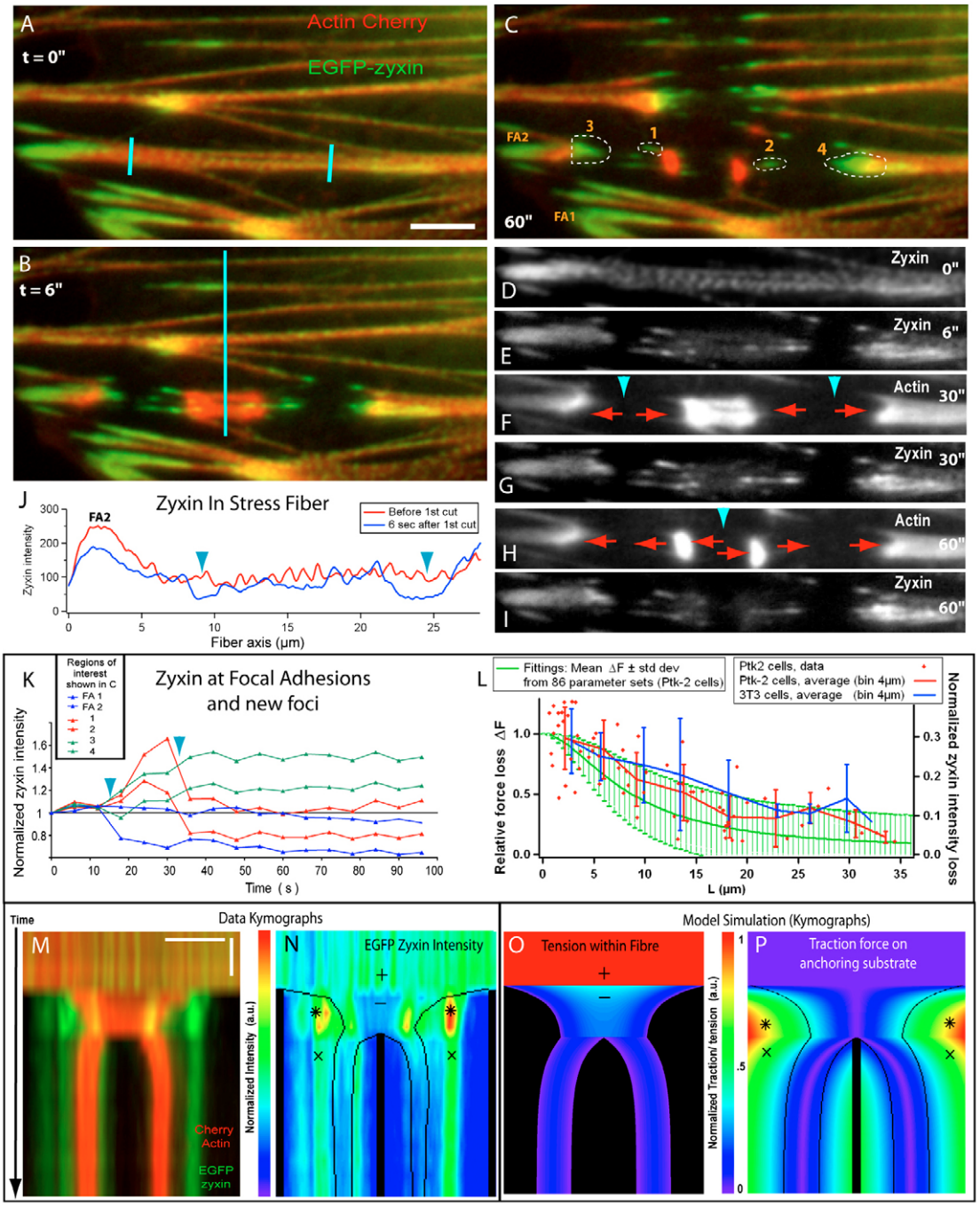

Fig. 3. Force correlates with protein localization along SFs. A Ptk-2 cell transfected with Cherry-zyxin and actin-EGFP constructs, before (A) and after (B,C) SF dissection (blue lines). (B) A 14 μm SF fragment is first released and retracts. (C) A second cut dissects the fragment, in its middle, and a neighbor control SF. (D) zyxin before cut, (E) zyxin 6 seconds after cut, (F,G) actin and zyxin 30 seconds after cut, (H,I) 30 seconds after second cut. Blue arrows indicate laser positions; red arrows indicate direction of retraction. The typical striated zyxin pattern (D) is lost instantaneously after release (E). (J) Intensity along the cut SF shows the loss of periodic signal along the SF axis in the 10-25 μm region. (K) Zyxin intensity in selected regions of C, numbered 1,2,3,4 for sites along SFs, and FA1 and FA2 for selected FA. Foci 1 and 2 (red) connected to the released fragment show fast enrichment of zyxin, which reverses after the second cut concomitantly with the reverse of actin movement (red arrows, see also M and supplementary material Movies 2-3). Foci 3 and 4 connected to outer retracting fibers undergo constant increase (green). FA2 (blue) shows important loss of zyxin, also visible in J, whereas the control FA is stable. (L) Zyxin intensity loss (right axis) at FAs connected to cut SFs, quantified in Ptk-2 cells (red, n=74 data points, segmented line: average ± s.d.) and 3T3 fibroblasts (blue, n=88, only average ± s.d.). The curves are in good agreement with the calculated force loss $\delta F(\kappa,L)$ (Appendix 1) obtained from the SF analysis in Fig. 2, which yielded 86 datasets and values of κ. The green curve shows the force loss average (± s.d.). (M) Double color kymograph of the central fiber fragment (red: actin, green: zyxin). (N) Intensity profile of the SF fragment, normalized and color coded according to the color scale (left of N). (O) Normalized calculated tension $\sigma(x,t)/\sigma_0$ within the SF fragment. (P) Traction $F_{trac}(x,t)$ normalized by maximal occurring value after cut (Appendix 1). The same normalized color scale applies to O and P. Symbols indicate common features in the experiments and the model. In O, tension is lost after cut (symbols + and –); in P, traction is built onto substrate crosslinkers (*) in a reversible manner after the second cut as shown by the subsequent loss (x). (O,P) contribute together to the observed zyxin intensity along the SF (N). Parameter values used in O and P are $(\kappa, \delta, \tau, \tau_\varepsilon) = (0.01, 0.70\,\mu m, 5\text{ seconds}, 0.1\text{ seconds})$. Kymographs M,N are interpolated. Scale bars: 5 μm (A); 5 μm horizontally, 10 minutes vertically (O). In both FAs and SFs, there is a general dynamic correlation between force and zyxin localization.

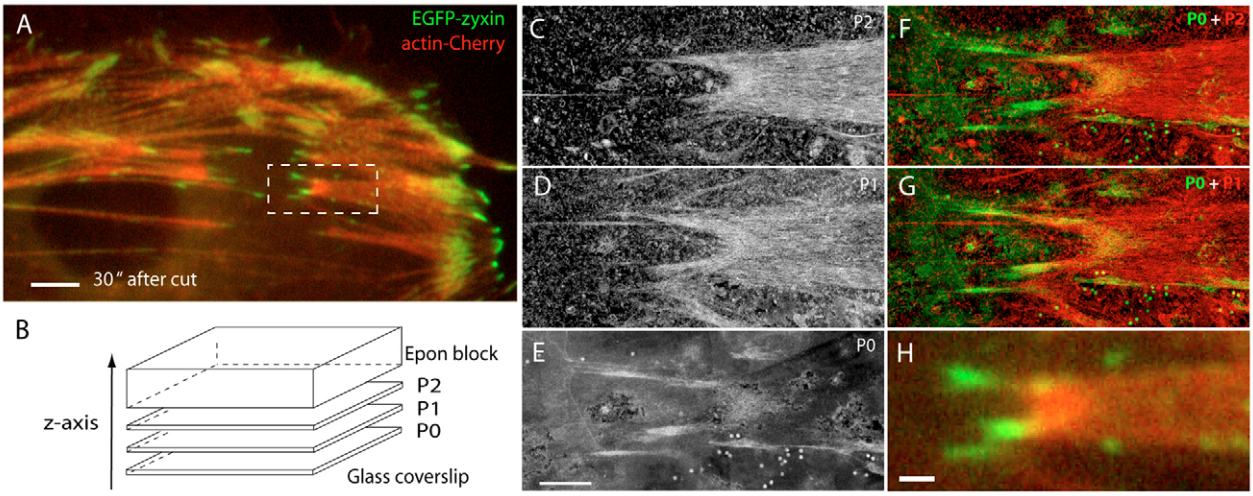

Fig. 4. Correlative TEM and fluorescent live microscopy shows that zyxin localizes at the basal membrane after cut. A Ptk-2 cell cotransfected with EGFP-zyxin and actin-Cherry constructs, 20 seconds after laser nanosurgery. (B) Schematic view of the Epon sectioning orientation. Plane P0 includes the basal side at the glass surface (0-50 nm), P1 the second (50-100) and P2 the third (100-150 nm). TEM views (inverted contrast) of the region in A (dashed rectangle): P2 in C, P1 in D, P0 in E. (F) Merged planes P0(green)+P1(red). (G) Merged planes P0(green)+P2(red). (H) Comparison of F and G to view fluorescent zyxin (green) and actin (red) in shows that zyxin localizes in the first section at the basal membrane. (Note that dot-like structures appearing sparsely in P0 are likely to be dirt particles on the Epon block surface.) Scale bars: 5 μm (A), 1.5 μm (E), 1 μm (H). See also supplementary material Fig. S2.

By performing correlative immunofluorescence, we compared vinculin distribution to the recruitment of zyxin along cut SFs. EGFP zyxin, expressed in the cell by transfection, is still detectable by fluorescence after fixation. Colocalization of vinculin with zyxin was observed nearly on all sites of newly recruited zyxin (supplementary material Fig. S3). Co-transfection of EGFP vinculin and cherry zyxin provided evidence that vinculin translocates to the same sites where zyxin is recruited, although in significantly smaller amounts (supplementary material Fig. S3). Of note, EGFP vinculin in living cells was not detected along SFs before dissection, nor was the vinculin antibody significantly along non cut fibers in fixed cells. These observations show that zyxin and vinculin are present at the formation of nascent adhesion sites induced by SFs sliding along the basal plasma membrane.

To address the spatial origin of the newly recruited zyxin, we dissected bleached SFs after performing complete photobleaching of their body, including FAs. We showed that the increase of zyxin signal at new sites of adhesions and the amount of zyxin lost from the connected FA after SF nanosurgery are not dynamically related, thereby demonstrating that zyxin is recruited from a pool source in the cytosol (see supplementary material Fig. S4 and Appendix 2).

Zyxin dynamics in *Drosophila* egg chamber epithelial tissue

To substantiate the relevance of the previous observations, we repeated laser nanosurgery experiments on the actin cytoskeleton in a living organism. We chose the follicular tissue of *Drosophila* egg chamber, which presents prominent and aligned actin bundles at its basal side. We generated transgenic lines expressing YPEt-zyxin to perform laser nanosurgery of actin bundles. Fig. 5 shows the relative distribution of YPet-zyxin (expressed) and actin (phalloidin fixation) in follicular cells at two different locations, basal (Fig. 5C-E) and apical (Fig. 5B). In the basal section, fluorescent zyxin bands appear all along actin bundles, and stronger patches align at the edge of the cell, very similarly to mature focal adhesions at the edge of cultured epithelial and fibroblastic cells. Fig. 5F-H) shows the cutting sequence on YPet-zyxin living cells (see also supplementary material Movie 4). A very fast retraction-like movement of zyxin patches is detectable after laser cut (supplementary material Movie 6). Immediately after cut, we also observe that opposing zyxin patches at the cell edge move roughly 1 μm apart (compared with an original separation of 20 μm), suggesting that tension along actin bundles is quickly released after cut. Subsequent to this, fast intensity loss from the zyxin patches at the edges of the cell could be verified, in contrast to control patches in neighbour cells (Fig. 5I), which showed random and weak fluctuations. Finally, we also observed large amounts of zyxin being recruited to discrete patches along the fiber close to the cutting edge, which were very similar to the foci previously described in cultured cells. The cells here were separate from the glass coverslip; however, an additional laminin membrane, called the basement membrane, surrounds the egg chamber and serves as the mechanical scaffold. These results suggest that zyxin behaves qualitatively and quantitatively very similarly along the actin bundles of a living epithelium and in SFs of cultured cells.

SF dynamics after myosin inhibition

We inhibited non-muscular myosin II activity with blebbistatin to confirm that the apparent translocation of zyxin from SF (Fig. 3) is due to a tension loss. Fig. 6 shows the change in zyxin intensity after blebbistatin treatment (10 μM) in Ptk-2 cells doubly transfected with actin-cherry and EGFP zyxin or with the α-actinin EGFP and cherry zyxin (supplementary material Movie 5). After 10 to 20 minutes in blebbistatin, the typical sarcomeric zyxin pattern vanished and the cytoplasmic intensity level increased (Fig. 6F,N). By contrast, actin and α-actinin patterns remained stable (Fig. 6H,P). Control experiments performed without fluorophore excitation to prevent phototoxicity of blebbistatin (Sakamoto et al., 2005) led to the same specific translocation of zyxin (data not shown) and control treatment with dimethylsulfoxide (DMSO) alone had no effect on zyxin localization (Fig. 6U). Moreover, after 20 minutes of blebbistatin treatment, we performed laser nanosurgery on SFs with actin-EGFP- and cherry-zyxin-transfected Ptk-2 cells. This resulted

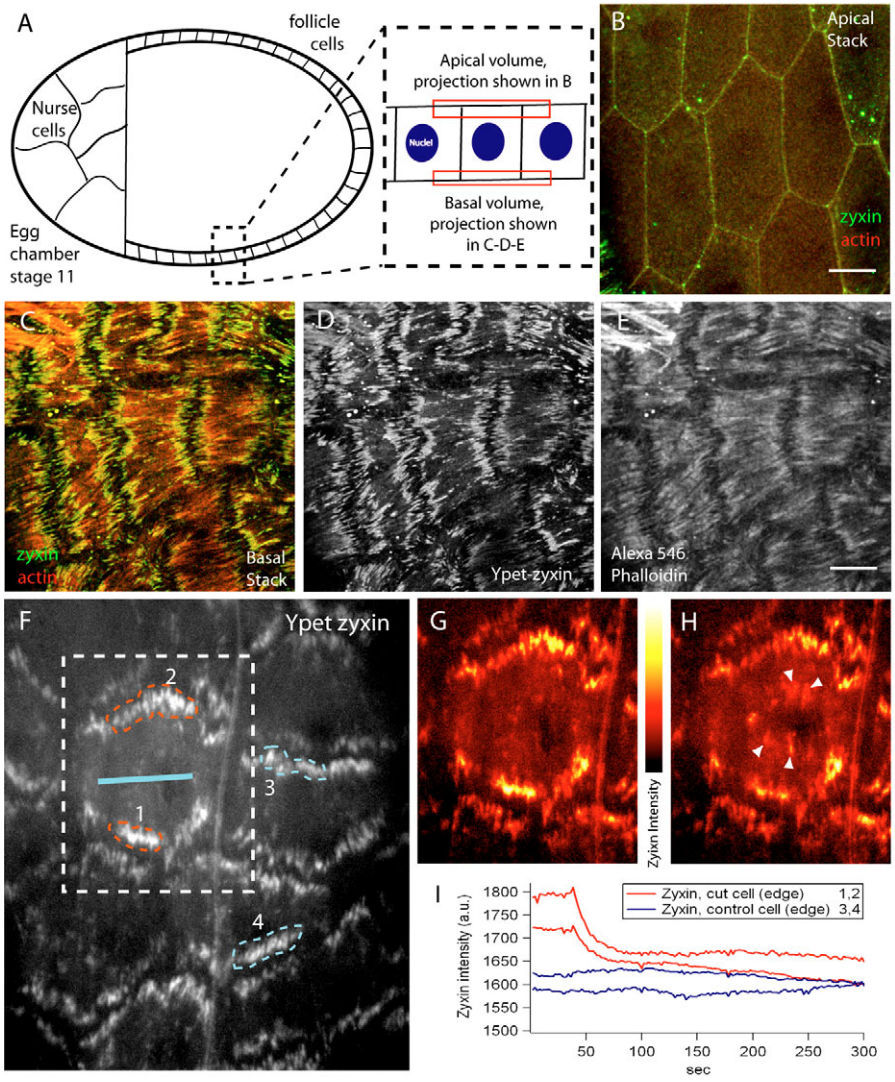

Fig. 5. The dynamics of zyxin along actin bundles in follicle cells of a *Drosophila* egg chamber. (A) Schematic view of a stage 11 egg chamber. (B) Polygonal organization of cells at apical side, axial projection of confocal stack. (C) Actin organization at the basal side. Actin-rich parallel bundles resemble SFs. (D,E) split channels with expressed Ypet-zyxin and red phalloidin staining. (F) Widefield fluorescent image of a live egg with Ypet-zyxin showing zyxin-rich areas along the cell outline. (G,H) Comparison of the cell intensity signal before and after laser surgery (blue target). Intensity is color-coded with the lookup table 'Red Hot' in ImageJ. A signal increase close to the cut is clearly shown in H, along the position of the actin bundles (white arrowheads). (I) Intensity dynamics of several areas, noted in F as areas 1,2,3 and 4. Areas belonging to the cut cell undergo a detectable decrease of fluorescence whereas control cells undergo random and weak fluctuations. See also supplementary material Movie 6. Scale bars: 10 µm (B,E).

in an immobile photobleached pattern on the SFs and a change in zyxin localization in the vicinity of the cut bundles was not observed (data not shown).

Reversible stretching of single SFs by AFM manipulation induces reversible recruitment of zyxin within SFs

We then investigated the effect of increasing external forces as applied specifically along SFs. To this end, we manipulated an AFM cantilever coated with fibronectin and set it in contact with the top of a Ptk-2 cell for 15 to 30 minutes to induce a connection with one or several basal SFs. After attachment to internal SFs, the cantilever was displaced along the direction of the fiber axis (see Materials and Methods). In supplementary material Movie 6, we show a cantilever pulling SFs three times over 2.5-3.5 µm in a cell expressing α-actinin-EGFP. The displacement of sarcomeric subunits was about 1.5 µm. The intensity of α-actinin along the pulled fiber tip (Fig. 7D) was unaffected during AFM manipulation. By contrast, the intensity of EGFP zyxin was strongly correlated with the cantilever movement. Mechanical forces were applied to two SFs periodically over nine cycles (see kymograph in Fig. 7C) and the load was applied over 10 seconds at each time. Fig. 7B shows two cycles of traction and release, on two SFs connected and displaced over 3 µm. The zyxin intensity increases during the traction phases along the front part of the SFs (see also supplementary material Movie 7) and drops subsequently upon SF release. By comparing the intensity increase of a pulled fiber and of a non-perturbed control SF within the same cell (Fig. 7D), we conclude that zyxin translocates along SFs according to the external load applied to it in a reversible manner. Interestingly, by plotting the intensity profile along one of the pulled fibers during a traction phase (Fig. 7E), we found that the intensity distribution of sarcomeric subunits increases specifically and locally, rather than in a continuous fashion.

Discussion

We have characterized with quantitative details the mechanical and mechanosensitive properties of SFs in living cells by combining laser nanosurgery, theoretical modeling, correlative live-cell and TEM imaging, and AFM. We used actin, α-actinin, zyxin and vinculin as fluorescent reporters of the mechanical state of SFs. Although earlier studies regarded zyxin as a focal adhesion marker, we showed that zyxin can be regarded more generally as a tension sensor related to the SFs where it localizes in a unique reversible manner to intracellular force nodes. Moreover, the active recruitment

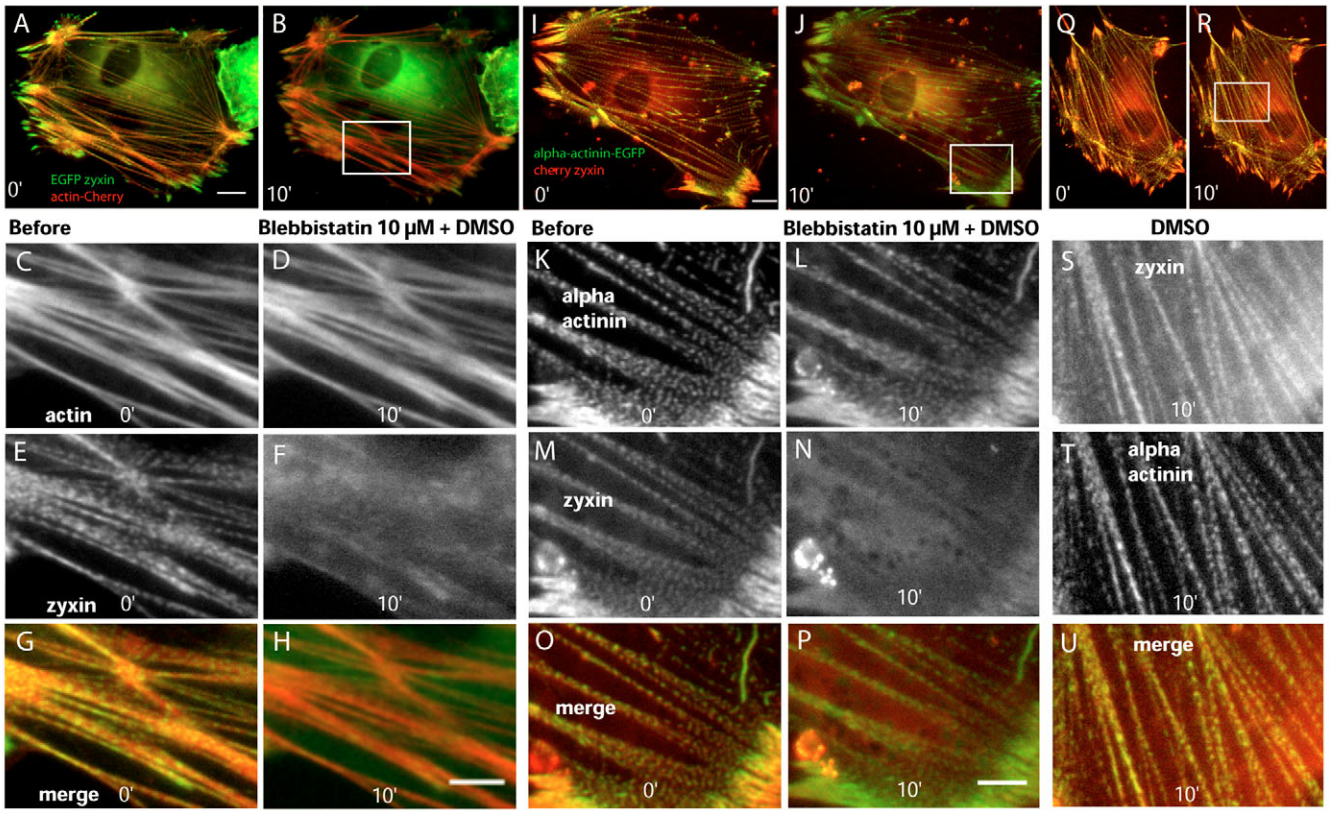

Fig. 6. Myosin-dependent localization of zyxin in SFs. Myosin II inhibitor blebbistatin (10 µM) was applied to Ptk-2 cells cotransfected with EGFP-zyxin and actin-Cherry (A-H) and with α-actinin-EGFP and Cherry-zyxin (I-P). (A,I) Overviews of the cells prior to treatment, (B,J) 10 minutes after treatment. (C-H,K-P) Closer view of the boxed areas. The initial sarcomeric localization of zyxin (E,M) vanishes (F,N) whereas actin SFs (C) and α-actinin (K) are stable 10 minutes after treatment (D,L). (Q-U) Control with DMSO only, showing no change in localization of zyxin and α-actinin. Scale bars: 10 µm (A-I), 5 µm (H-P). See also supplementary material Movie 7.

of zyxin at the interface between retracting SFs and the plasma membrane has demonstrated a new mechanosensitive mechanism of adhesion formation induced by intracellular forces.

Our analysis of SF laser retraction dynamics provides the experimental basis to validate a precise mechanical model, including its stationary and dynamic solutions. In particular, our model explains the peculiar observation that SFs contract non-uniformly along their length. Recently, the contraction of SFs was analyzed with a simpler viscoelastic model that regards SFs as a single loaded spring connecting FAs (Kumar et al., 2006). Such a model, however, could not account for the non-uniform contraction of sarcomeric units reported here. In our study, we account for the contractile actomyosin forces explicitly and have not to assume a pre-strain of SFs. Furthermore, we prove that the SF is coupled to its environment. By evaluating the impact of non-endogenous expression of α-actinin on the degree of crosslinking κ, we showed that α-actinin significantly influences κ, and therefore is a good candidate for the crosslinker. This finding is consistent with the multiple roles and binding properties of α-actinin (for a review, see Otey and Carpen, 2004), which links actin to integrins and vinculin.

Regarding the nature of the crosslink, it is very likely that intermediate contacts to the glass substrate, similarly to small integrin clusters undetectable by fluorescence microscopy, underlie the SFs and are responsible for the mechanical coupling. In fact, the plasma membrane itself cannot provide mechanical anchorage because of its fluid nature. Another candidate could be a crosslinkage of SFs to the surrounding actin cytoskeleton. If such a link had a relevant mechanical impact on SF dynamics, however, we should have observed several phenomena. For example, side by side dissected SFs would tend to pull on each other and to retract with similar dynamics; by contrast, we observed that neighboring SFs could retract independently, as shown in supplementary material Movie 2. Also, with links to the surrounding cytoskeleton, retracting SFs would apply forces to lateral positions, away from their original axis. By contrast, we observed zyxin relocalization only in certain positions along the axis. Finally, TEM data did not reveal actin filaments extending away from the axis of SFs. In conclusion, we believe that the major mechanical connection is to the substrate at the basal membrane. Consistent with this, nanosurgery experiments in *Drosophila* egg chambers have shown similar anchorage of actin bundles, away from a glass interface. In egg chambers, epithelial cells are in contact with an external basement membrane (Horne-Badovinac and Bilder, 2005), which could provide sufficient mechanical support. This transmembrane linkage could function in a similar way to that observed in muscle cells, where costameres (α-actinin-rich protein complexes) connect sarcomeres and extracellular matrix and thereby transmit forces to the cellular environment (Ervasti, 2003).

The mechanical interaction of SFs through the basal membrane with the substrate allowed us to observe a new mechanism for adhesion formation. The simultaneous relocalization of zyxin and small amounts of the adhesion protein vinculin along the path of

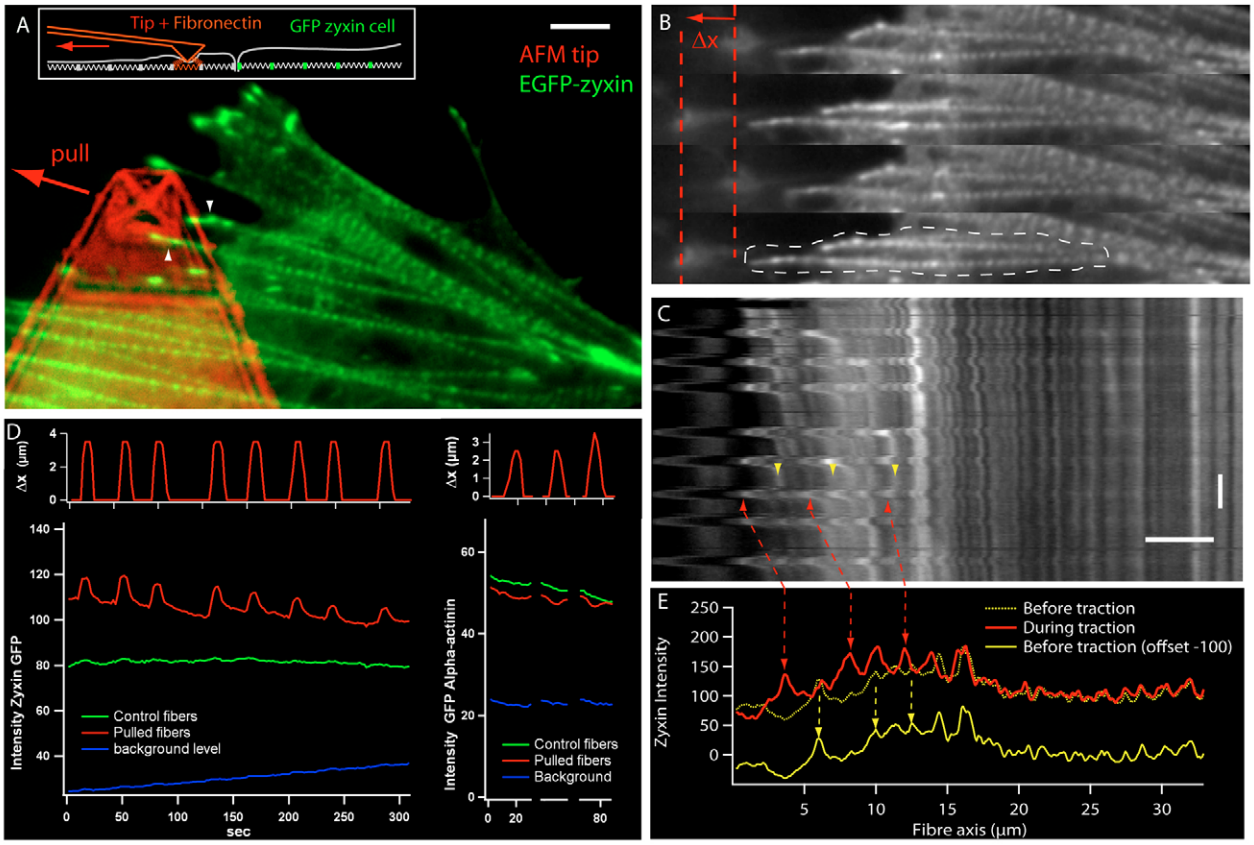

Fig. 7. Acute recruitment of zyxin on single SFs pulled with an AFM cantilever. (A) Position of the fibronectin-coated AFM cantilever, extracted from a transmission micrograph taken before traction, overlapped with a EGFP-zyxin-expressing Ptk-2 cell. In inset, schematic side view of the manipulation experiment with the AFM tip in orange, applied from the top and connecting to basal SFs through the membrane. Springs represent SF subunits. Traction applies to the neighboring cell's SFs and propagates to fluorescent SFs of interest through cell-cell junctions (white arrows). Two fibers are periodically pulled over a distance Δx (See supplementary material Movie 7). (B) Relaxed and pulled fibers during two different cycles. (C) Kymograph showing the full traction sequence over nine cycles. (D) Zyxin intensity increase over time (left, red) compared with a control fiber (green). Δ*x* was manually measured from the kymograph. The total cell intensity was corrected for bleaching (see background in blue). The intensity of pulled and control SFs in α-actinin-expressing cells (right, see supplementary material Movie 6), showing no correlation between the traction (top) and the intensity of the SFs. (E) Intensity profile of the seventh traction plotted before traction (dashed yellow, reported with offset in plain yellow because of overlap) and during the traction (red). Before traction, the typical sarcomeric labeling of zyxin is clearly visible from the intensity profile with, on average, 1 μm periodic ripples. After traction, the amplitude of the ripples increases in the front stretched part of the fiber, thereby showing a discrete and periodic recruitment of zyxin along the bundle. Scale bars: 5 μm (A-C) horizontal, 40 seconds vertical (C).

SF retraction has demonstrated the formation of nascent adhesion structures in response to SF retraction. It is a challenge to ensure that vinculin recruitment is not an artifact; however, we showed previously (Colombelli et al., 2007) that SF nanosurgery did not impair nor influence plasma membrane integrity and membrane protein diffusion. Therefore, we believe that vinculin recruitment here is part of the mechanosensitive mechanism.

From this and from the TEM data, we conclude that when actin filaments slide along the membrane (pulled here by myosin motors) they trigger adhesion formation. This result is consistent with recent studies where external forces and FA dynamics correlate. For example, Riveline and colleagues (Riveline et al., 2001) showed the enhanced growth of pre-existing FAs under external forces exerted by micropipettes. The biochemical activity, studied on stretched cells, provided details about the molecular mechanisms by which external forces could induce changes within FAs. A concept of 'substrate priming' was proposed (Sawada et al., 2006) by which phosphorylation activity in FAs could be promoted when proteins come closer to each other or mechanically unfold in response to external mechanical force. However, no study has so far reported the formation of an adhesion contact triggered by pure mechanical friction of actin filaments along the plasma membrane. Instead, recent studies have shown the different levels of dynamic correlation between integrins, FA-related proteins such as vinculin and talin, and actin filaments (Guo and Wang, 2007; Brown et al., 2006; Hu et al., 2007). The hierarchical organization of FAs therefore constitutes a differential 'slippage-clutch' mechanism (Wang, 2007), which transmits forces from actin motion to the extracellular matrix to promote cell migration (Hu et al., 2007). A vice-versa mechanism would explain how cells sense external stress transmitted to the actin cytoskeleton (Yoshigi et al., 2005). Here, we showed that actin motion along the membrane transmits mechanical force to the extracellular matrix by triggering adhesion formation. It is likely that a similar mechanosensitive mechanism, stimulated by actin-filament sliding, also occurs in living tissues, as opposed to cells cultured on glass. Evidence for this is the strong quantitative similarity we have measured between the recruitment dynamics of zyxin in the *Drosophila* egg chamber and in cultured cells. This could be a key mechanism in the field of cell migration where the combinatorial and hierarchical relation between actin polymerization,

actin movement and FA formation is not yet fully understood. The retrograde meshwork flux of polymerized actin filaments in the lamellipodium could in fact induce FA formation and trigger on its own the forward propulsion necessary for cell movement.

Finally, we have shown a dual localization of zyxin at FAs and SFs in correlation with tension and traction forces, which raises central questions about the mechanism of zyxin localization and its role. In particular, we showed that a considerable fraction of fluorescent zyxin is instantaneously released from FAs (up to 40%, Fig. 3) as well as from SFs (virtually all, Figs 3 and 6) after SF tension relaxation. In previous studies, pharmaceutical treatment to inhibit contractility showed delocalization of zyxin away from FAs (Guo and Wang, 2007; Lele et al., 2006), whereas other FA components like vinculin did not show such behavior after similar treatment. Also, its unbinding rate increased in FAs after SF dissection (Lele et al., 2006). Consistent with this, we observed that the turnover of zyxin in FAs decreases threefold after SFs release (supplementary material Fig. S4). However, we showed that zyxin localization is also tension dependent along SFs (Figs 3 and 7). Thus, could there be a single mechanism underlying zyxin recruitment at FAs and SFs? Moreover, if zyxin behaves as a mechanical tension sensor, what would be the recruiting mechanical switch? The zyxin primary structure is known (Smeichel et al., 1998), and its major binding partner is α-actinin (Crawford et al., 1992; Reinhard et al., 1999; Li and Trueb, 2001). Interestingly, the binding site on α-actinin involves two spectrin-like subdomains (Djinovic-Carugo et al., 2002) and interaction occurs only when α-actinin dimerizes (Li and Trueb, 2001). Spectrin domains are also known to have unique flexible properties (Mirijanian and Voth, 2008). In this study, we have shown that SFs are strongly attached through the basal plasma membrane, where zyxin senses the tension built by actin movement. We showed that α-actinin is involved in this mechanical coupling. Moreover, we observed that the periodic colocalization zyxin and α-actinin vanishes instantaneously after releasing SF fragments (Fig. 3), and that zyxin is recruited reversibly along pulled SFs in a discontinuous and periodic manner (Fig. 7). In FAs, we have shown an instantaneous loss of zyxin after tension release and also shown that α-actinin is a major candidate for crosslinking SFs to FAs (Zaidel-Bar et al., 2007). Altogether, this experimental evidence supports a crucial role of α-actinin in regulating the force-dependent localization of zyxin in FAs and SFs.

In Fig. 8, we depict a hypothetical mechanism explaining the possible dual recruitment mechanism of zyxin by α-actinin in SFs and FAs. In SFs, the antiparallel movement of actin filaments creates forces on α-actinin dimers that crosslink them. Actin filament sliding along FAs, also noted as retrograde flux, could exert forces onto α-actinin, the linker between actin and FAs. A plausible mechanically induced conformational change of the dimer could increase the susceptibility of zyxin binding. The flexibility of spectrins and their redundant organization along α-actinin (eight domains in a dimer) could therefore serve as a docking platform, which mechanically regulates the number and activity of zyxin-binding sites. Further analysis of zyxin and α-actinin-binding partners will be necessary to determine the exact number of proteins involved in the mechanical switch and the role of its mechanosensing nature. However, it is worth mentioning that genetic knockout of zyxin (Hoffmann et al., 2006) or RNAi suppression (Harborth et al., 2001) have been shown to suppress the formation of SFs in fibroblasts, or to impair cytoskeletal reinforcement (Yoshigi et al., 2005). Within SFs, we showed that zyxin is a molecular sensor that identifies the location of forces and tensions. In answer to those intracellular cues, and in combination with a yet unknown number of partners, it could trigger specific mechanisms to counteract and equilibrate mechanical imbalances within the cytoskeleton, for instance by influencing actin polymerisation, as suggested recently (Hitara et al., 2008).

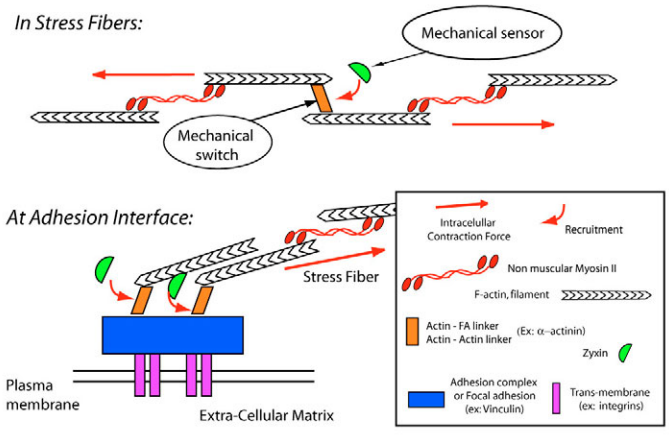

Fig. 8. Possible mechanism of mechanosensing in SFs. Zyxin is recruited along actin bundles and FAs by mechanical force increase. In SFs, the opposite contraction force (red arrows) applied by myosin II induces the opposite movement of antiparallel actin filaments, which could be transduced to the actin-actin crosslinker α-actinin. A conformational change or binding properties modifications could allow zyxin recruitment. At FAs (bottom left), the same contraction movement can propagate to α-actinin, which links actin filaments and FA proteins such as vinculin. The mechanical switch regulating zyxin recruitment could have the same force-transduction mechanism with the same molecule, for example α-actinin, in SFs and FAs.

Materials and Methods

Laser nanosurgery and microscopy

Intracellular dissection of SFs was performed by low energy plasma ablation (Vogel and Venugopalan, 2003), with a pulsed UV laser [470 picoseconds per pulse, 355 nm (Colombelli et al., 2004)]. Plasma membranes do not undergo detectable damage after dissection of basal SFs, as shown previously (Colombelli et al., 2007). Nanosurgery was performed at 100-500 pulses per second with a density of 5.5 pulses/μm and energy of 50 nJ per pulse to reach a dissection accuracy of 450 nm, as shown previously (Colombelli et al., 2005). Fluorescent imaging was performed on a regular inverted microscope with a Hamamatsu ORCA camera. Frame rate varied from 0.5-1 second with a Zeiss 63×/1.2 water-immersion lens and around 1 second with an Olympus 150×/1.45 oil-immersion lens. In double-color mode, it takes about 7 seconds to acquire one image. FRAP or photobleaching was performed with a free-space-coupled multiline Argon ion laser. Laser nanosurgery in *Drosophila* was performed with identical parameters as in cultured cells.

Image processing

Kymographs were constructed with ImageJ. Multiple edge detection (programmed in Matlab) of bleached actin GFP or α-actinin in SFs was performed on kymographs by extracting multiple maxima positions of the derivative of the intensity profile along the SFs. When needed, kymographs were smoothed in the distance direction. Intensity measurements of zyxin at FAs and along SFs were performed in ImageJ on manually designed, closed regions of interest. FRAP quantification was performed with Igor Pro, based on a regular FRAP analysis procedure (Phair et al., 2004). The average width of striated subunits was evaluated by counting the total number of subunits (n=1595), divided by the total length (along 95 SFs), which does not reflect the intrinsic variation from the SFs periphery to the centre shown in Peterson et al. (Peterson et al., 2004). See Appendix 1 for details of statistical analysis.

Cell culture, transfections and chemicals

G-Actin-GFP plasmids originate from Alen Piljic (EMBL, Heidelberg, Germany), cherry constructs from Roger Tsien (UCSD, La Jolla, CA). EGFP-zyxin, cherry-zyxin, actin-cherry and EGFP-vinculin were cloned in the labs of Klemens Rottner and Vic Small. α-actinin-EGFP was constructed by Jurgen Wehland (HZI, Braunschweig, Germany). Ptk-2 and Swiss 3T3 cells were seeded on live cell dishes (MatTek, MA)

in modified Eagles medium (MEM, Gibco) and Dulbecco's-MEM (Life Technologies, Karlsruhe, Germany) respectively, with 10% fetal calf serum for Ptk-2 and 10% newborn calf serum for Swiss 3T3 cells with 1% penicillin-streptomycin and 1% L-glutamine. Cells were transfected when covering 70% of the culture surface (preparation in 2 ml medium: plasmids 1 μg/dish and 3 μl FuGene 6 Transfection Reagent from Roche, Indianapolis, IN). Cells were imaged between 14 and 20 hours after transfection. Blebbistatin (Sigma) was diluted in DMSO and applied at 10 μM during fluorescent acquisition. For each experiment described, five cells were studied and showed consistent results.

Drosophila cloning and imaging of egg chambers

We produced a *Drosophila* transformation vector containing a N-terminal YPet (Rizzo et al., 2004) tagged Zyx102EF, *Drosophila* zyxin orthologue (Renfranz et al., 2003). YPet was amplified from the pLNCyPetMAMM plasmid to generate a DNA fragment with a *Bgl*II cohesive 5′ and a *Eag*I cohesive 3′ end. Zyx102EF was amplified from the BDGP DGC clone LD06023 (Rubin et al., 2000) in order to generate a DNA fragment with a *Eag*I cohesive 5′ and a *Xho*I cohesive 3′ end. Both DNA fragments were cloned into the *Bgl*II-*Xho*I-cleaved pUAST vector, generating pUAST-YPet-zyxin. Transgenic lines were generated using standard procedures. A recombinant *Drosophila* line carrying tubP-GAL4 (Bloomington *Drosophila* Stock Center) and UAS-YPet-zyxin on the third chromosome was generated by recombination.

Ovaries expressing YPet-zyxin under tubulin promoter control were dissected from adult females in Schneider medium. The ovarioles were mounted between a glass coverslip and a gas-permeable plastic foil (bioFOLIE 25, In Vitro System and Services, Göttingen, Germany). Living follicular cells were imaged and laser dissected in egg chambers at stage 11. Actin staining of follicular cells expressing YPet-zyxin under tubulin promoter control were dissected in PBS and fixed in 4% formaldehyde PBS. Actin was stained with Alexa Fluor 546-Phalloidin (Invitrogen, Molecular Probes). The ovarioles were mounted in Vectashield (Vector Laboratories). Stained follicular cells at stage 11 egg chambers were imaged on a Leica TCS-SP5.

Correlative immunofluorescence and electron microscopy

Laser surgery was used to mark the location of the cell of interest (Colombelli et al., 2008) before imaging and fixation with paraformaldehyde (3%). Immunolabelling was performed with a monoclonal anti-zyxin antibody (Biozol-Abcam, Munich, Germany), a monoclonal anti-vinculin antibody (hVIN-1, Sigma). We fixed cells for electron microscopy (solution: 2.5% glutaraldehyde, 50 mM cacodylate buffer, 2% sucrose, 0.05 M KCl, 0.4 mM $MgCl_2$, 0.04 mM $CaCl_2$) within 10 seconds of imaging for 30 minutes at room temperature, they were then washed with 50 mM cacodylate buffer (5 times 2 minutes), kept on ice during incubation with postfixation solution (2% OSO_4, 50 mM cacodylate buffer) for 40 minutes, rinsed in H_2O and incubated in 0.5% uranyl acetate in H_2O for 30 minutes before rinsing and embedding. Flat embedding was carried out in Epon (Serva, Heidelberg, Germany) and samples were sectioned 40-50 nm thick. The glass surface was laser etched after fixation to mark the cell position and to form Epon ridges, visible under stereomicroscopy for precise trimming (Colombelli et al., 2008).

AFM micromanipulation

A JPK Nanowizard atomic force microscope (JPK Instruments, Berlin, Germany), interfaced onto an Axiovert 200 (Carl Zeiss, Göttingen, Germany) equipped with an incubator chamber (CellBiology Trading, EMBL, Hamburg), was used to mechanically stimulate the cells and to define the horizontal path for the cantilever to follow. Tipless Silicon nitride cantilevers (NP-0, Veeco Instruments, Dourdan, France) were washed in a piranha solution (H_2O_2/H_2SO_4, 30-70%), rinsed with Milli-Q water and treated with oxygen plasma for 5 minutes and incubated in a 0.1 mg/ml fibronectin (Sigma) PBS solution for 1 hour at room temperature. The fibronectin-coated cantilever was positioned in contact with the apical plasma membrane to create contact exactly above a SF, observed in fluorescence. After 15 to 30 minutes, the cantilever eventually formed a strong adhesion site connecting the cantilever and the SF (supplementary material Movie 6), or the SF of a neighbor cell connecting a fluorescent SF through a cell-cell junction (supplementary material Movie 7). The fiber was then stretched by driving the cantilever along a line path aligned with the axis of the SF, with a constant velocity of 1 μm/second along 2 to 4 μm.

Appendix 1

Stress fiber model

We present a minimal model for SFs that takes into account the internal visco-elastic and contractile properties of the fiber (Besser and Schwarz, 2007) as well as viscoelastic interactions with its surrounding. From the discrete description (supplementary material Fig. S5), we derive a partial differential equation which describes SF contraction dynamics. The model is solved numerically. Solutions are compared with experimental time-dependent displacement fields along SFs after laser surgery. Despite its simplicity, the model fits the dynamic contraction of several sarcomeric units along a SF. By using the model, we are able to extract the mechanical parameters of SFs. Furthermore, the model provides an estimate of the tension within the SFs and the forces on the FAs that are not accessible experimentally with our set-up. In this way, we can correlate zyxin localization with mechanical forces and quantify its mechanosensitivity.

The SF is modelled as a linear chain of Kelvin-Voigt bodies (Fung, 1993) that consist of a dashpot with viscosity γ_{int} and a spring of stiffness k_{int} connected in parallel. These two modules represent the internal viscous and elastic properties of the SF, respectively. We introduce into these Kelvin-Voigt bodies a further contractile element that represents the activity of motor proteins. Its properties are given by the specific force-velocity relation of the molecular motors. Experimental observation showed that SFs contract non-homogeneously after laser dissection (Fig. 1). This behavior can be explained by mechanical interactions of the SFs with their surrounding. Thus, in the model we account for mechanical crosslinks by harmonic restoring forces, denoted by springs of stiffness k_{ext} and introduce an external viscosity γ_{ext} due to the viscous drag within the cytosol. According to the discrete picture depicted in supplementary material Fig. S5, we describe the force F_n at the site n as the sum of all spring forces, viscous drags and forces F_m of motor proteins:

$$F_n = \gamma_{int}\partial_t\left(u_{n+1}-u_n\right)-\gamma_{int}\partial_t\left(u_n-u_{n-1}\right)+k_{int}\left(u_{n+1}-u_n\right) -k_{int}\left(u_n-u_{n-1}\right)-\gamma_{ext}\partial_t u_n-k_{ext}u_n+F_{m_{n+1}}-F_{m_n}\ . \quad \text{(A1)}$$

The first two terms account for internal friction due to relative filament sliding. These two discrete forces depend on the contraction velocity of neighboring sites $\partial_t(u_{n+1}-u_n)$. The next two terms account for elastic forces within the SF and depend on the relative displacement of neighboring sites ($u_{n+}1-u_n$). The contributions from viscous drag within the cytosol depend on the local retraction velocity $\partial_t u_n$. The harmonic restoring forces due to the mechanical cross-links depend on the local displacement u_n of the considered site. The last two terms account for the contractile forces resulting from molecular motor activity, which we describe for simplicity by a linear force-velocity relationship:

$$F_m = F_{stall}\left(1-\frac{v}{v_0}\right)\ . \quad \text{(A2)}$$

F_m is the actual force exerted by a motor moving with velocity v. v_0 is the zero-load velocity and F_{stall} is the stall force of the motor. The continuum approximation of Eqn A1 is given by:

$$F(x,t) = a^2\gamma_{int}\Delta\dot{u}(x,t)+a^2k_{int}\Delta u(x,t)-\gamma_{ext}\dot{u}(x,t) -k_{ext}u(x,t)+a\nabla F_m(x,t)\ . \quad \text{(A3)}$$

We use the fact that the motor force F_m depends on the displacement $u(x,t)$. The contraction δ_n within the nth element generated by the respective motor is given by $\delta_n=-(u_n-u_{n-1})$. The contraction velocity is therefore $v(x,t)=\dot{\delta}(x,t)\approx-a=\nabla\dot{u}(x,t)$ and the force velocity relation Eqn A2 is given by:

$$F_m(x,t) = F_{stall}\left(1+\frac{a\nabla\dot{u}(x,t)}{v_0}\right)\ . \quad \text{(A4)}$$

This relation together with the assumption that internal and external forces have to balance, $F(x,t)=0$ (there are no other forces acting on the SF), leads to a continuous model for the SF:

$$a^2\Delta u(x,t)+\tau a^2\Delta\dot{u}(x,t)-\kappa u(x,t)-\tau_\varepsilon\dot{u}(x,t)=0\ . \quad \text{(A5)}$$

We define the stiffness ratio $\kappa=k_{ext}/k_{int}$, which can be regarded as a measure for the degree of crosslinking. In addition, we introduce the two time scales $\tau=(\gamma_{int}+F_{stall}/v_0)/k_{int}$ and $\tau_\varepsilon=\gamma_{ext}/k_{int}$. The SF model equation (Eqn A5) can be solved numerically. The imposed initial conditions are an unperturbed SF at the beginning: $u(x,t=0)\equiv 0$. The appropriate boundary conditions are zero displacement for the one end of the SF, which is clamped by focal adhesions, $u(x=0,t)\equiv 0$, and we impose zero tension boundary conditions for the other end where the SF is dissected:

$$\tau a\nabla\dot{u}(L,t)+a\nabla u(L,t)+\delta=0\ . \qquad \text{(A6)}$$

L is the initial length of the considered fiber fragment and we define the contraction length $\delta=F_{stall}/k_{int}$. Owing to the linear force-velocity relationship, the motor contribution decomposes into two parts. On one hand, it adds up to the internal viscosity (see expression for τ in Table A1) and thus slows down the equilibration process. On the other hand, the stall force of the motors appears in the boundary condition (see contraction length δ in Eqn A6) and can be regarded as a pre-strain.

Data fitting and analysis

The set of equations, consisting of the model for the time-dependent displacement field $u(x,t)$ along the SF Eqn A5 together with the appropriate boundary conditions Eqn A6 are solved numerically with the MATLAB pde toolbox function 'parabolic' (version 1.0.4) and fitted to the experimentally measured first three bands of the kymographs. In this way, we restrict the fitting to a 10-μm-large region of the SF where most of the contraction happens. Bands that are further away from the cut are rather stationary and do not provide distinct information. As fit routine, we use the function 'lsqnonlin' of the MATLAB optimisation toolbox (version 3.0), which is a specialized algorithm to solve nonlinear least-squares data-fitting problems. To check for local minima, we start the global optimization algorithm ten times with random initial sets of positive parameter values $(\kappa,\delta,\tau,\tau_\varepsilon)$. For virtually all SFs and all runs the algorithm converges to the same fiber specific least-squares minimum defining one set of parameter values $(\kappa,\delta,\tau,\tau_\varepsilon)$. In total we analyzed 86 SFs from actin-transfected cells and 34 SFs from α-actinin-transfected cells. From fits to these data sets we were able to deduce the distributions of the four parameters for both transfection methods. Mean values and standard deviations are summarized in Table A1. We find an average stiffness ratio $\kappa=0.035\pm0.034$ (values are given as mean ± s.d. or denoted otherwise) for actin-transfected cells, which indicates that the stiffness of the SF exceeds the elastic contributions from crosslinks by a factor of roughly 30. The average contraction length of a sarcomeric unit (of initial width a=1 μm) is about $\delta=0.66\pm0.36$ μm. This comes close to the 380 nm measured length of multiple antiparallel myosin chains in smooth muscle cells (Trybus and Lowey, 1987), suggesting that SFs subunits have a surprisingly wide contractile range (66% of equilibrium length 1 μm). The typical timescale for contraction is dictated by internal processes, that is relative filament sliding and motor activity and amounts to $\tau=29\pm27$ seconds. The second time scale resulting from drag within the cytosol is considerably smaller $\tau_\varepsilon\ll\tau$ and can been neglected without loss of generality, see also the discussion of model parameters below.

The parameter values for the α-actinin transfected cells are of similar magnitude; however, the mean values of the two parameters κ and τ differ significantly from the respective values obtained from actin-transfected cells. In order to compare the parameter samples from the actin- and the α-actinin-transfected cells we applied a Student's t-test for differences of the means. The t-test analysis shows that the crosslink parameter κ is significantly higher (t-test: P=0.0000014) and the time scale τ is significantly lower (t-test: P=0.0029) for the α-actinin-transfected cells. The remaining parameters δ and τ_ε are independent of the transfected protein. Transfections of EGFP α-actinin and actin GFP induce an overexpression of non-endogenous proteins, whose level can be monitored with the overall fluorescence of individual cells. (In our experiments, only low expressing cells were selected.) It is known that α-actinin acts as a crosslinker between actin filaments and also connects SFs to integrin-mediated adhesion clusters through the FA core protein vinculin. According to the model, higher values for the cross-link parameter κ reflects a higher level of mechanical crosslinks of SFs to the surroundings. These results thus suggest that α-actinin is a potential candidate as a mechanical crosslinker. It could reflect attachment of SFs either to secondary actin cytoskeletal network or, and most likely according to us, to intermediate contacts to the substrate such as integrin clusters; however, in amounts that are difficult to detect by fluorescence.

By contrast, the difference in the time scale $\tau=\gamma_{int}/k_{int}+\delta/v_0$ according to the transfection method, lacks a simple explanation. The contraction length of sarcomeric units δ is independent of the transfection (compare values in Table A1) and we assume the same for the maximal velocity of the motors v_0. Therefore, in terms of our simple model, we conclude that the ratio of internal friction over fiber stiffness γ_{int}/k_{int} is reduced when α-actinin is overexpressed.

Stationary solution

Once cut, and for times $t\gg\tau$, the SF approaches a new mechanical equilibrium. The model simplifies to a second order ordinary

Table A1. Model parameter interpretations and values obtained from fits to the data

Parameter	Abbreviation for	Interpretation	Actin-FRAP Mean ± s.d.	α-actinin Mean ± s.d.	P-value (t-test)
κ	k_{ext}/k_{int}	Crosslink ratio	0.035±0.034	0.078±0.059	0.0000014
δ	F_{stall}/k_{int}	Contraction length	0.66±0.36 μm	0.59±0.33 μm	0.35
τ	$(\gamma_{int}+F_{stall}/v_0)/k_{int}$	Equilibration time	29±27 seconds	15±11 seconds	0.0029
τ_ε	γ_{ext}/k_{int}	Equilibration time	0.13±0.23 seconds	0.15±0.27 seconds	0.72

Actin-FRAP n=86 SFs, α-actinin n=34 SFs. κ denotes the dimensionless ratio of stiffness of the crosslinks over stiffness of the SF. δ is the contraction length in μm of a sarcomeric unit. τ is the time scale in seconds associated with effective internal friction including motor contributions, whereas τ_ε is the time scale associated with external friction. We provide the mean and s.d. for each model parameter. To compare the parameter distributions for the actin-FRAP and the α-actinin data we applied a Student's t-test analysis. The crosslink parameter κ results significantly higher and the time scale τ significantly lower for the α-actinin-transfected cells. The remaining parameters are independent of the transfection method. Furthermore, we find that $\tau_\varepsilon\ll\tau$.

differential equation that can be solved analytically for the stationary state after retraction.

$$a^2 \Delta u_{ss}(x) - \kappa u_{ss}(x) = 0 \ , \qquad \text{(A7)}$$

with the boundary conditions $u_{ss}(0)=0$ at the end where the SF is clamped by focal adhesions and $a^2=u_{ss}(L)+\delta=0$ at the end where the SF is cut. The solution for the stationary state displacement is given by:

$$u_{ss}(x) = -\frac{\delta}{\sqrt{\kappa}} \frac{\sinh(\sqrt{\kappa}\, x / a)}{\cosh(\sqrt{\kappa}\, L / a)} \ . \qquad \text{(A8)}$$

For $\kappa \to 0$ this relation simplifies to $u_{ss}(x)=-\delta x/a$. The contraction becomes uniform along an uncrosslinked SF, which leads to a displacement linear in x. However, if $\sqrt{\kappa} \gg a/L$, the stationary solution Eqn A8 is approximated by:

$$u_{ss}(x) \approx -\frac{\delta}{\sqrt{\kappa}} \exp\left(\sqrt{\kappa}\,(x-L)/a\right) . \qquad \text{(A9)}$$

Thus, the mechanical perturbation of cutting a crosslinked SF decays exponentially from the cut edge on a typical length scale given by $a/\sqrt{\kappa}$. As a consequence, with a fiber fragment length $L \gg a/\sqrt{\kappa}$, the internal part of the fiber close to the FA remains unaffected by the nanosurgery. In particular, the force exerted by the SF on the adhesion is unchanged (see below). Assuming $\kappa=0.035$ and $a=1$ μm, we find that this typical length scale amounts to $a/\sqrt{\kappa} \approx 5.4$ μm for actin-transfected cells, and $a/\sqrt{\kappa} \approx 3.6$ μm for α-actinin-transfected cells.

Total retraction length

Eqn A8 also provides the total retraction of the SF after equilibration as a function of the initial fiber length L:

$$\Delta L(L) = \left| u_{ss}(L) \right| = \frac{\delta}{\sqrt{\kappa}} \tanh(\sqrt{\kappa}\, L / a) \ . \qquad \text{(A10)}$$

Each parameter set $(\kappa, \delta, \tau, \tau_\varepsilon)$ obtained from fits to kymographs provides one curve $\Delta L(L)$. In order to compare the model prediction with the measured data we average 86 curves obtained from actin transfected cells and 34 curves obtained from α-actinin transfected cells. In Fig. 2E (main text) we show the sample average model curve $\langle \Delta L(L) \rangle_{actin}$ with the s.d. for the data obtained from actin-transfected cells. For the limiting case where $L \gg a/\sqrt{\kappa} \approx 5.4$ μm, the total retraction becomes constant $\Delta L \approx \delta/\sqrt{\kappa}$, and is therefore independent of L. This agrees with the experimentally measured retraction length, which is constant for SFs larger than 10 μm$>a/\sqrt{\kappa}$. For comparison, we include the expected dependence of the total retraction length assuming a completely uncrosslinked SF, $\Delta L(L)=\delta \cdot L/a$, deduced from Eqn A10 when $\kappa \to 0$, shown as a black solid line in Fig. 2E. The respective quantities for α-actinin-transfected cells are shown in supplementary material Fig. S1D. By comparing the results shown in Fig. 2E and supplementary material Fig. S1D, one finds that the total contraction length is persistently lower for α-actinin transfected cells. This is due to higher values for the crosslink parameter κ in this sample. The other relevant parameter δ is independent of the transfection method and thus does not contribute to the differences.

Forces on FAs

The fluorescence intensity of zyxin in FAs decreases when the associated SF is dissected by the laser pulses. The loss of intensity, however, depends on the precise location of the cut. As shown in Fig. 3L, the relative loss of intensity $\delta I_{rel}=(I_0-I_{ss})/I_0$ is maximal when the cut is applied close to the focal adhesion and decreases with increasing distance between cut and FA. This can be understood quantitatively by the model assuming that the intensity of zyxin is proportional to the force exerted on the focal adhesion. The relative force loss at the boundary is defined as:

$$\delta F_{rel} = \frac{F_0 - F_{ss}}{F_0} \ . \qquad \text{(A11)}$$

We assume that the SF is in mechanical equilibrium prior to the cut, that is, all motors operate at their stall force, $F_0=F_{stall}$. The force on the FA in the new mechanical equilibrium after cut F_{ss} is given by:

$$F_{ss} = a k_{int} \nabla u_{ss}(x=0) + F_{stall} \ . \qquad \text{(A12)}$$

Together with the derivative of Eqn A8 we find for the relative force loss at the FA:

$$\delta F_{rel}(L) = 1 / \cosh(\sqrt{\kappa}\, L / a) \ . \qquad \text{(A13)}$$

The relative force loss at the FA depends only on the crosslink parameter κ and the initial length of the fiber fragment L. In accordance with Eqn A9 we find that the mechanical integrity around the focal adhesion remains unperturbed when $L \gg a/\sqrt{\kappa}$. In Fig. 3L, we show the sample average curve for the expected relative force loss, $\langle \delta F_{rel}(L) \rangle_{actin}$, compared with the measured relative intensity loss of zyxin at FAs in actin-transfected cells. The agreement between model and experimental data suggests that the zyxin concentration in FAs depends on the applied force.

Tension in SFs and traction forces on the substrate

From the discrete representation in supplementary material Fig. S5, one can deduce the tension in the SF as:

$$\sigma(x,t) = a\gamma_{int} \nabla \dot{u}(x,t) + a k_{int} \nabla u(x,t) + F_m(x,t) \ . \qquad \text{(A14)}$$

Using Eqn A4 and using the definition of the parameters τ and δ yields:

$$\sigma(x,t) / k_{int} = a\tau \nabla \dot{u}(x,t) + a \nabla u(x,t) + \delta \ . \qquad \text{(A15)}$$

In the following, we use Eqn A15 to calculate the tension within the SF. In Fig. 3O (main text) we show the normalized tension $\sigma(x,t)/\sigma_0$,where $\sigma_0=F_{stall}$ is the constant tension in the SF prior to the cut. After the cut, the tension within the fiber fragment quickly drops to low values. Simultaneously, the zyxin striated pattern along the SF is exposed to a quick intensity loss (compare + and – symbols in Fig. 3N,O). In Fig. 3P, we plot the traction force exerted by a crosslink on the substrate at its anchor point, given by $F_{trac}(x,t)/k_{int}=-\kappa u(x,t)$. A comparison of the traction force (Fig. 2N) and the zyxin intensity (Fig. 3N) suggests that after the cut, zyxin relocalizes in regions where crosslinks become highly tensed by the retracting SF.

Discussion of model parameters

We finally discuss the importance of the four model parameters δ, κ, τ and τ_ε. The parameter δ, describing actomyosin contractility, is obviously essential to reproduce the retraction of the SF. For instance, $\delta \to 0$ together with the initial condition $u(x,t=0) \equiv 0$ lead to the trivial solution $u(x,t) \equiv 0$.

From the stationary model Eqn A7, we can deduce that a vanishing crosslink parameter, $\kappa \to 0$, implies that $-\nabla u(x)=const$. The negative gradient of the displacement, however, is a measure for the relative change in density within the SF, which is found to be

constant. In other words, each sarcomeric unit along the SF would finally contract to the same extent, irrespective of the parameters τ and τ_ε, which dictate the dynamics of the contraction. This finding explains the final collapse of the curves in supplementary material Fig. S6K for t>120 seconds, where external crosslinks were neglected. By contrast, the experimental results show that the contraction of sarcomeric units is inhomogeneous along the SF: the subunit closest to the cut shows the largest contraction and the sarcomeric contraction length decrease with increasing distance from the cut (compare supplementary material Fig. S6D and Fig. S6K). Additionally, from Eqn A8 we deduce that the steady state displacement of the sarcomeres, for $\kappa\rightarrow 0$, is proportional to their position: $u_{ss}(x)=-\delta\cdot x/a$. For example, the final displacement of the sarcomere in the middle of the SF is expected to be 50% of the displacement of the fiber tip, irrespective of the total length of the SF. However, we found experimentally that sarcomeres located several microns away from the cut, remain unaffected (see bands in supplementary material Fig. S6B in the range of x=0...15 μm). The model with $\kappa\rightarrow 0$ is thus not able to reproduce the experimental kymographs.

A model neglecting internal friction, with $\tau\rightarrow 0$, fails to correctly reproduce the dynamics of the contraction. Although the long term behavior (supplementary material Fig. S6F) is captured by the model, it fails to reproduce the contraction dynamics shortly after cut (supplementary material Fig. S6G). In particular, the retraction of the inner bands is delayed compared to the ones closer to the cut (compare black and blue model curve in supplementary material Fig. S6G). This is in contrast to the experimental data that shows the central bands to react fastest (compare black and blue data in supplementary material Fig. S6G). This discrepancy between the model with $\tau\rightarrow 0$ and experimental data becomes even more apparent in the analysis of the normalized sarcomere width (supplementary material Fig. S6H).

In contrast to the model parameters δ, κ and τ, which are essential to understand the retraction dynamics of the SF, we found empirically that the equilibration time τ_ε originating from external friction plays a minor role compared to the internal equilibration time τ. From the extracted parameter values summarized in Table A1, one finds that $\tau_\varepsilon/\tau<O(10^{-2})$. The equilibration dynamics of the SFs are thus dominated by the time scale of the internal processes and the term proportional to τ_ε can be neglected in good approximation. The simplified model including only the three parameters δ, κ and τ provides in general a fit of similar quality. For the experimental data analyzed in supplementary material Fig. S6A-D, the simplified model gives the same fit results as the full model.

Appendix 2

To address the spatial origin of the newly recruited zyxin, we combined photobleaching, FRAP and nanosurgery experiments. We quantified the fluorescent recovery of FAs after FRAP and compared the half-life $t_{1/2}$ to the increase of zyxin fluorescence in foci along SF after cut. Zyxin relocalization at foci ($t_{1/2}$=12.9±5.5 seconds, n=16) showed approximately 2.5-fold faster kinetics than a regular FA recovery ($t_{1/2}$=32.9±10.0 seconds, n=24, see the Materials and Methods for kinetics quantification). We then applied laser dissection onto SFs that were fully photobleached and compared zyxin recovery at FAs and at new foci (supplementary material Movie 5). Zyxin relocalized more than threefold faster at foci ($t_{1/2}$=29.1±12.6 seconds, n=34) than in FAs ($t_{1/2}$=95.1±71.8 seconds, n=27). Interestingly, we observed that the fluorescence levels at zyxin foci raised above the initial fluorescent level of zyxin at SFs before dissection, indicating the creation of new recruitment sites after SF retraction, in contrast to a regular fluorescence recovery. Altogether, these data show that there is no correlation between loss of zyxin from FAs and new recruitment at foci, i.e. zyxin is newly recruited from the cytosol rather than from the perturbed SFs and their connected FAs, and therefore reacts on a cellular level within the whole cell.

We thank Gunter Stier, Andrea Parmeggiani, Ada Cavalcanti-Adam and Francesco Pampaloni for discussions and interest; Claude Antony for technical support in EM experiments; Joachim Spatz for technical support in AFM; Alfons Riedinger and Georg Ritter from EMBL workshops for technical help with instrumentation; Brigitte Joggerst, Stefanie Benesch, Massimiliano Mazza, Sasa Mendjan and Rainer Pepperkok for help and reagents; and Jan Kaluza from Olympus ODE Germany for the loan of components.

References

Besser, A. and Schwarz, U. S. (2007). Coupling biochemistry and mechanics in cell adhesion: a model for inhomogeneous stress fiber contraction. *New J. Phys.* **9**, 425.

Brown, C. M., Hebert, B., Kolin, D. L., Zareno, J., Whitmore, L., Horwitz, A. R. and Wiseman, P. W. (2006). Probing the integrin-actin linkage using high-resolution protein velocity mapping. *J. Cell Sci.* **119**, 5204-5214.

Chrzanowska-Wodnicka, M. and Burridge, K. (1996). Rho-stimulated contractility drives the formation of stress fibers and focal adhesions. *J. Cell Biol.* **133**, 1403-1415.

Colombelli, J., Grill, S. W. and Stelzer, E. H. K. (2004). Ultraviolet diffraction limited nanosurgery of live biological tissues. *Rev. Sci. Instrum.* **75**, 472-478.

Colombelli, J., Reynaud, E. G., Rietdorf, J., Pepperkok, R. and Stelzer, E. H. K. (2005). *In vivo* cytoskeleton dynamics quantification in interphase cells induced by UV pulsed laser nanosurgery. *Traffic* **6**, 1093-1102.

Colombelli, J., Reynaud, E. G. and Stelzer, E. H. K. (2007). Investigating relaxation processes in cells and developing organisms: from cell ablation to cytoskeleton nanosurgery. *Methods Cell Biol.* **82**, 267-291.

Colombelli, J., Taengemo, C., Haselmann-Weiss, U., Anthony, C., Stelzer, E. H. K., Pepperkok, R. and Reynaud, E. G. (2008). A correlative light and electron microscopy method based on laser micropatterning and etching. *Methods Mol. Biol.* **457**, 203-213.

Crawford, A. W., Michelsen, J. W. and Beckerle, M. C. (1992). An interaction between zyxin and α-actinin. *J. Cell Biol.* **116**, 1381-1393.

Djinovic-Carugo, K., Gautel, M., Ylänne, J. and Young, P. (2002). The spectrin repeat: a structural platform for cytoskeletal protein assemblies. *FEBS Lett.* **513**, 119-123.

Ervasti, J. M. (2003). Costameres: the Achille's heel of Herculean muscle. *J. Biol. Chem.* **278**, 13591-13594.

Fung, Y. C. (1993). *Biomechanics: Mechanical Properties of Living Tissues*. New York: Springer Verlag.

Gillespie, P. G. and Walker, R. G. (2001). Molecular basis of mechanosensory transduction. *Nature* **413**, 194-202.

Guo, W. and Wang, Y. L. (2007). Retrograde flux of focal adhesion proteins in response to cell migration and mechanical signals. *Mol. Biol. Cell* **18**, 4519-4527.

Harborth, J., Elbashir, S. M., Bechert, K., Tuschl, T. and Weber, K. (2001). Identification of essential genes in cultured mammalian cells using small interfering RNAs. *J. Cell Sci.* **114**, 4557-4565.

Hitara, H., Tatsumi, H. and Sokabe, M. (2008). Mechanical forces facilitate actin polymerization at focal adhesions in a zyxin-dependent manner. *J. Cell Sci.* **121**, 2795-2804.

Hoffmann, L. M., Jensen, C. C., Kloeker, S., Albert Wang, C. L., Yoshigi, M. and Beckerle, M. (2006). Genetic ablation of zyxin causes Mena/VASP mislocalization, increased motility, and deficits in actin remodeling. *J. Cell Biol.* **172**, 771-782.

Horne-Badovinac, S. and Bilder, D. (2005). Mass transit: epithelial morphogenesis in the *Drosophila* egg chamber. *Dev Dyn.* **232**, 559-574.

Hotulainen, P. and Lappalainen, P. (2006). Stress fibers are generated by two distinct actin assembly mechanisms in motile cells. *J. Cell Biol.* **173**, 383-394.

Hu, K., Ji, L., Applegate, K. T., Danuser, G. and Waterman-Storer, C. M. (2007). Differential transmission of actin motion within focal adhesions. *Science* **315**, 111-115.

Kim-Kaneyama, J. R., Suzuki, W., Ichikawa, K., Ohki, T., Kohno, Y., Sata, M., Nose, K. and Shibanuma, M. (2005). Uni-axial stretching regulates intracellular localization of Hic-5 expressed in smooth-muscle cells *in vivo*. *J. Cell Sci.* **118**, 937-949.

Kumar, S., Maxwell, I. Z., Heisterkamp, A., Polte, T. R., Lele, T. P., Salanga, M., Mazur, E. and Ingber, D. E. (2006). Viscoelastic retraction of single living stress fibers and its impact on cell shaoe, cytoskeletal organization, and extracellular matrix mechanics. *Biophys. J.* **90**, 3762-3773.

Lele, T. P., Pendse, J., Kumar, S., Salanga, M., Karavitis, J. and Ingber, D. E. (2006). Mechanical forces alter zyxin unbinding kinetics within focal adhesions of linving cells. *J. Cell. Physiol.* **207**, 187-194.

Li, B. and Trueb, B. (2001). Analysis of the α-actinin/zyxin interaction. *J. Biol. Chem.* **276**, 33328-33335.

Martinac, B. (2004). Mechanosensitive ion channels: molecules of mechanotransduction. *J. Cell Sci.* **117**, 2449-2460.
Mirijanian, D. T. and Voth, G. A. (2008). Unique elastic properties of the spectrin tetramer as revealed by multiscale coarse-grained modeling. *Proc. Natl. Acad. Sci. USA* **105**, 1204-1208.
Mitra, S. K., Hanson, D. A. and Schlaepfer, D. D. (2005). Focal adhesion kinase: in command and control of cell motility. *Nat. Rev. Mol. Cell. Biol.* **6**, 56-68.
Morris, C. E. (1998). Mechanosensitive ion channels in eukaryotic cells. In *Cell Physiology Source Book*, 2nd edn (ed. N. Sperelakis), pp. 668-681. San Diego CA: Academic Press.
Nix, D. A. and Beckerle, M. C. (1997). Nuclear-cytoplasmic shuttling of the focal contact protein, zyxin: a potential mechanism for communication between sites of cell adhesion and the nucleus. *J. Cell Biol.* **138**, 1139-1147.
Otey, C. A. and Carpen, O. (2004). α-actinin revisited: a fresh look at an old player. *Cell Motil. Cytoskeleton* **58**, 104-111.
Pellegrin, S. and Mellor, H. (2007). Actin stress fibers. *J. Cell Sci.* **120**, 3491-3499.
Peterson, L. J., Rajfur, Z., Maddox, A. S., Freel, C. D., Chen, Y., Edlund, M., Otey, C. and Burridge, K. (2004). Simultaneous stretching and contraction of stress fibers *in vivo*. *Mol Biol. Cell.* **15**, 3497-3508.
Phair, R. D., Gorski, S. A. and Misteli, T. (2004). Measurement of dynamic protein binding to chromatin *in vivo*, using photobleaching microscopy. *Methods Enzymol.* **375**, 393-414.
Reinhard, M., Zumbrunn, J., Jacquemar, D., Kuhn, M., Walter, U. and Trueb, B. (1999). An α-actinin binding site of zyxin is essential for subcellular zyxin localization and α-actinin recruitment. *J. Biol. Chem.* **274**, 13410-13418.
Renfranz, P. J., Siegrist, S. E., Stronach, B. E., Macalma, T. and Beckerle, M. C. (2003). Molecular and phylogenetic characterization of Zyx102, a Drosophila orthologue of the zyxin family that interacts with Drosophila enabled. *Gene* **305**, 13-26.
Riveline, D., Zamior, E., Balaban, N. Q., Schwartz, U. S., Ishizaki, T., Narumiya, S., Kam, Z., Geiger, B. and Bershadsky, A. D. (2001). Focal contacts as mechanosensors: externally applied local mechanical force induces growth of focal contacts by an mDia1-dependent and ROCK-independent mechanism. *J. Cell Biol.* **153**, 1175-1185.
Rizzo, M. A., Springer, G. H., Granada, B. and Piston, D. W. (2004). An improved cyan fluorescent protein variant useful for FRET. *Nat. Biotechnol*. **22**, 445-449.
Rubin, G. M., Hong, L., Brokstein, P., Evans-Holm, M., Frise, E., Stapleton, M. and Harvey, D. A. (2000). A Drosophila complementary DNA resource. *Science* **287**, 2222-2224.
Sakamoto, T., Limouze, J., Combs, C. A., Straight, A. F. and Sellers, J. R. (2005). Blebbistatin, a myosin II inhibitor, is photoinactivated by blue light. *Biochemistry* **44**, 584-588.
Sawada, Y., Tamada, M., Dubin-Thaler, B. J., Cherniavskaya, O., Sakai, R., Tanaka, S. and Sheetz, M. P. (2006). Force sensing by mechanical extension of the Src family kinase substrate p130Cas. *Cell* **127**, 1015-1026.
Smeichel, K. L., Stronach, B. E. and Beckerle, M. C. (1998). Purification and assay of zyxin. *Methods Enzymol.* **298**, 62-76.
Trybus, K. M. and Lowey, S. (1987). Assembly of smooth muscle myosin minifilaments: effects of phosphorylation and nucleotide binding. *J. Cell Biol.* **105**, 3007-3019.
Vogel, A. and Venugopalan, V. (2003). Mechanisms of pulsed laser ablation of biological tissues. *Chem. Rev.* **103**, 577-644.
Vogel, V. and Sheetz, M. (2006). Local force and geometry sensing regulate cell functions. *Nat. Rev. Mol. Cell. Biol.* **7**, 265-275.
Wang, Y. L. (2007). Flux at focal adhesions: slippage clutch, mechanical gauge, or signal depot. *Sci STKE*, pe10.
Wang, Y., Botvinick, E. L., Zhao, Y., Berns, M. W., Usami, S., Tsien, R. Y. and Chien, S. (2005). Visualizing the mechanical activation of src. *Nature* **434**, 1040-1045.
Yoshigi, M., Hoffman, L. M., Jensen, C. C., Yost, H. J. and Beckerle, M. C. (2005). Mechanical force mobilizes zyxin from focal adhesions to actin filaments and regulates cytoskeletal reinforcement. *J. Cell Biol.* **171**, 209-215.
Zaidel-Bar, R., Milo, R., Kam, Z. and Geiger, B. (2006). A paxillin tyrosine phosphorylation switch regulates the assembly and form of cell-matrix adhesions. *J. Cell Sci.* **120**, 137-148.
Zaidel-Bar, R., Itzkovitz, S., Ma'ayan, A., Iyengar, R. and Geiger, B. (2007). Functional atlas of the integrin adhesome. *Nat. Cell Biol.* **8**, 858-867.

Journal of Cell Science